


 Cite this: *RSC Adv.*, 2025, 15, 49320

# Advances in surface-enhanced Raman scattering applications for precision agriculture: monitoring plant health and crop quality

Ha Anh Nguyen, \* Dao Thi Nguyet Nga, To Dao Cuong, Mai Quan Doan and Anh-Tuan Le \*

Ensuring plant health and crop quality is vital for sustainable modern agriculture. Conventional detection methods for stress markers, contaminants, and pathogens are often constrained by labor-intensive procedures, bulky equipment, and reliance on centralized facilities, limiting real-time field monitoring. Surface-enhanced Raman scattering (SERS) has emerged as a promising solution, providing rapid, ultrasensitive, and non-destructive analysis across plant, soil, and water matrices. This review outlines the fundamental SERS mechanisms and strategies that boost sensing performance, and surveys recent advances in monitoring throughout the cultivation cycle, covering plant stress markers, metabolites, contaminants, and plant pathogens under realistic agricultural conditions. Emphasis is placed on substrate architecture (hot-spot control, composites/heterostructures, functionalization, flexible formats), enhancement mechanisms, and analytical performance (typical enhancement factor (EF), limit of detection (LOD), limit of quantitation (LOQ), and relative standard deviation (RSD) ranges). Persistent challenges, including substrate reproducibility, matrix interference, quantitative calibration, and scalable fabrication for field deployment, are evaluated alongside emerging solutions, including matrix-aware calibration (with ratiometric readout), fluorescence-robust preprocessing, and durable, large-area platforms. We close with practical considerations for durability and cost and with future perspectives toward next-generation, field-ready SERS tools for proactive plant-health management and crop-quality assurance.

 Received 3rd November 2025  
 Accepted 3rd December 2025

DOI: 10.1039/d5ra08452k

[rsc.li/rsc-advances](https://rsc.li/rsc-advances)

## 1. Introduction

Agriculture in general, and cultivation in particular, have played a vital role throughout human history. Cultivation is the backbone of global food production, providing grains, fruits, vegetables and livestock feed. Therefore, as the population grows, development in cultivation is essential to ensure food security and meet the increasing food demands. Besides, crops such as cotton, rubber and sugar canes are key materials for industries and food processing. Medicinal plants are essential for pharmaceutical and cosmetic production. Moreover, in many countries, farmers cultivate crops such as tea, coffee, cocoa, and palm oil for exportation, which is a great contribution into the overall economy of the countries. Thus, cultivation has provided employment and livelihoods for a significant portion of the population. Therefore, plant health and crop quality have been well-concerned for years. In the past, farmers tried to protect their crops from pests and weeds using pesticides and herbicides. However, pesticides have been reported to cause stress on

plant health and enhance crop resistance.<sup>1</sup> Moreover, overusing pesticides and herbicides reduces the quality of the crops and leads to a risk in food safety. Consuming grains, fruit and vegetables containing those residues might lead to accumulation of these contaminants in human bodies and cause diseases.<sup>2</sup> On the other hand, to provide more nutrients for plants, farmers have utilized fertilizers for their crops. Nevertheless, the use of fertilizers may lead to soil salinization and acidification, resulting in water stress and ion antagonism.<sup>3</sup> Therefore, modern agriculture recommends using technology and data analysis to observe, measure and respond to variability in crops to adjust agricultural inputs such as water, fertilizer and pesticides to optimized yield, minimize waste and enhance sustainability. It is called precision agriculture,<sup>4</sup> in which plant health and crop quality monitoring is required to provide data for farmers to optimize those inputs.

Plant health has been assessed using several methods, including visual, biochemical, and molecular techniques. In the field, farmers have been using traditional methods based on their experiences. They usually observe plant leaves to find chlorosis (yellow leaves), necrosis (dead tissue) and wilting, which can indicate as signs of drought, nutrient deficiency or even infections. However, these symptoms are not specific. The

*Phenikaa University Nano Institute (PHENA), Phenikaa School of Engineering (PSE), Phenikaa University, Hanoi 12116, Vietnam. E-mail: anh.nguyenha@phenikaa-uni.edu.vn; tuan.leanh@phenikaa-uni.edu.vn*



overlapping symptoms could easily lead to misdiagnosis, resulting in inappropriate treatment.<sup>5</sup> In addition, the symptoms could only be observed at late stages, reducing the effectiveness of intervention.<sup>6</sup> Instead, biochemical and molecular methods have been developed for more specific detection of plant conditions of stress. Plant stress can be divided into biotic stress or infection, which are caused by pathogenic fungi, bacteria or viruses, and abiotic stress, which is the result of drought, severe temperature and salinity. Both biotic and abiotic stresses on plants lead to changes in quantities of different molecules inside or released from plants, including phytohormone, reactive oxygen species (ROS), volatile organic compounds (VOCs), *etc.* Therefore, to monitor plant health, researchers have developed various methods to detect pathogen and stress-related molecules.<sup>6</sup> To detect pathogenic microorganisms, pathogen isolation<sup>7</sup> and enzyme-linked immunosorbent assay (ELISA)<sup>8</sup> are specific. However, pathogen isolation is time-consuming while ELISA is not sensitive at early stages of infection. Molecular techniques such as polymerase chain reaction (PCR) and quantitative PCR could be overcome that disadvantage as they allow deoxyribonucleic or ribonucleic acid (DNA/RNA) of the pathogens to be amplified to be detected at low levels.<sup>9</sup> However, they require expensive equipment and reagents, and complicated prior processing of DNA/RNA extraction. For stress-related molecules, molecules in plants can be detected using chromatography,<sup>10</sup> gas chromatography-mass spectrometry (GC-MS),<sup>11,12</sup> spectrophotometry<sup>13</sup> and tissue staining.<sup>14</sup> In spite of accuracy, they are time-consuming and need extensive sample preparation. Precious agriculture, however, requires fast and accurate measurements to update plant health, allowing farmers to determine the stress of plants and the reason for those stress conditions to adjust the inputs.

In addition to in-season monitoring, ensuring optimal crop quality requires attention at both the earliest and latest stages of production. Pre-cultivation assessment of agricultural soils and irrigation water is essential for identifying potential hazards, such as heavy metal ions, pesticide residues and other contaminants, that can compromise plant growth and enter the food chain. Likewise, pre-harvest monitoring serves as a critical final safeguard, enabling detection of residual agrochemicals and pathogenic infections in leaves, fruits, and flowers. Traditional analytical techniques, such as chromatography coupled with mass spectrometry and enzyme-linked immunoassays, offer high accuracy and multiplexed detection capabilities. For example, GC-MS-based metabolomics has been widely employed to profile plant metabolites, identifying hundreds of compounds including sugars, amino acids, and organic acids.<sup>15</sup> Liquid chromatography (LC)- and GC-MS untargeted metabolomics have also revealed shifts in soil metabolites under continuous cultivation stress in ramie crops.<sup>16</sup> Multi-residue pesticide quantification methods using “Quick, Easy, Cheap, Effective, Rugged and Safe” (QuEChERS) extraction and LC-MS/MS have been validated for soil analysis, achieving sub-nanogram-per-gram sensitivity in field samples.<sup>16</sup> However, these methods frequently require labor-intensive sample preparation, bulky instrumentation, and centralized laboratory infrastructure, which limit their suitability for real-time, in-field

applications. Integrating sensitive, rapid, and non-destructive analytical approaches at both pre-cultivation and pre-harvest stages, along with cultivation period, is therefore central to achieving safe, high-quality, and sustainable agricultural production.

Surface-enhanced Raman Spectroscopy (SERS) is a powerful analytical technique that significantly amplifies the Raman signal of the analytes adsorbed on nanostructure metallic surfaces, allowing detection of chemical and biological molecules at trace levels.<sup>17–19</sup> Raman scattering is an inelastic light-matter interaction, in which incident photons interact with molecular vibrations, resulting in the shift in energy of the photons. Therefore, the Raman shifts refer to unique vibration frequencies of the molecules. As each chemical bond and functional group has characteristic vibrational energies, the resulting Raman spectrum serves as a molecular “fingerprint” which identifies the molecule.<sup>20–22</sup> Despite excellent specificity, the Raman scattering effect is weak, which limits its application.<sup>21</sup> As an extension of conventional Raman spectroscopy, SERS retains the specificity of Raman scattering while overcoming its weakness thanks to plasmon-mediated enhancement. By adsorbing analyte molecules onto or near the surface of noble metal nanostructures such as silver (Ag), gold (Au), or copper (Cu) nanoparticles (NPs), the Raman signal of the molecules is enhanced *via* two main mechanisms: electromagnetic and chemical enhancements. On one hand, localized surface plasmon resonance (LSPR) occurs on the surface of the NPs due to the oscillation of free electrons under laser excitation. This results in local field enhancement, which amplifies the Raman signal through the electromagnetic mechanism (EM).<sup>21</sup> On the other hand, the Raman enhancement observed in SERS phenomenon is also attributed to the chemical mechanism (CM), which involves charge transfer (CT) between the substrate and the analytes. This process alters the electron density distribution within the molecules, increasing their polarizability and thereby enhancing the Raman scattering signal.<sup>23</sup> Hence, SERS excels in delivering both rapid and highly accurate molecular detection, making it particularly advantageous for plant health and crop quality monitoring.

Among plant-related analytes, pesticides are the most common target for SERS thanks to their structures with various functional groups, allowing them to be adsorbed directly onto metallic structures to experience SERS effects. Several reviews have been established about those SERS sensors, focusing on agri-food safety.<sup>24–26</sup> However, the scope of SERS analytes in plant health and crop quality monitoring has been broadening beyond pesticide residues. Many SERS sensors have been developed to detect various compounds in plants, vegetables, and fruits, including plant stress markers (*e.g.*, phytohormones, secondary metabolites, ROS, VOCs), other metabolites, pesticides, *etc.* as well as in agricultural water and soil matrices such as metal ions, nanoparticles, micro-nanoplastics, *etc.* These analytes provide valuable insights into crop growth stages, abiotic stress, or pathogen infection, enabling precision agriculture practices such as targeted irrigation or nutrient supplementation.



This review shifts the emphasis from cataloging surface-enhanced Raman scattering (SERS) examples to quantitative performance in realistic agricultural matrices. We bring together recent work (with greater weight on studies since 2020) across mechanisms and substrate engineering (*i.e.*, hot-spot control, composites, functionalization, flexible formats) and anchor it to applications in residue screening, volatile organic compound (VOC) phenotyping, and pathogen detection. Rather than isolated demonstrations, we extract design rules linking geometry, composition, and surface chemistry to measurable precision, and conclude topic blocks with concise enhancement factor (EF)/relative standard deviation (RSD)/limit of detection (LOD) summaries to guide method selection. We also synthesize practical remedies for recurrent failure modes (fluorescence/daylight background, hot-spot stochasticity, stability, matrix interference) and outline field-deployment practices, including matrix-matched or standard-addition calibration with ratiometry and reported baselining; external checks at decision levels and against regulatory comparators (*e.g.*, maximum residue limits (MRLs), World Health Organization/Food and Agriculture Organization (WHO/FAO) water limits); and durability/sustainability elements (stabilized surfaces, shelf-life reporting, indicative cost-per-test, biobased supports). We also trace how SERS aligns with agricultural stages, from pre-season water/soil screening, through in-season plant-stress and pathogen surveillance, to harvest-time residue checks and post-harvest quality/authenticity control, so laboratory sensitivity can translate into reliable, comparable evidence for agricultural decisions.

## 2. SERS mechanisms and keys to optimize SERS sensing performance

Since its discovery, Raman spectroscopy (RS) has proven its ability to generate molecular fingerprint spectra, in which distinct peaks correspond to specific vibrational modes. However, the applications of RS are limited by the intrinsic low efficiency of Raman scattering. Compared to the efficiency of other processes such as fluorescence emission ( $\sim 10^{-16}$  cm<sup>2</sup> per cr) and infrared absorption ( $\sim 10^{-20}$  cm<sup>2</sup> per cr), this value of Raman scattering is only  $10^{-30}$  cm<sup>2</sup> per cr,<sup>27</sup> thus, it requires long acquisition times or high laser powers achieve acceptable signal-to-noise ratio. This excitation can damage the analytes. Besides, many organic compounds emit fluorescence under light excitation, which can overwhelm the Raman signal, so it can be difficult to interpret their Raman spectra. Therefore, RS is not such a powerful analytical tool. However, with the assistance of metallic nanostructures on which analyte molecules are adsorbed, Raman signal can be enhanced by  $10^{14}$ – $10^{15}$  fold in SERS effect,<sup>28</sup> allowing it to overcome the main drawback of RS to become a great tool for analytical applications. In this section, the mechanism of SERS will be discussed to clarify the strategies to optimize the performance of SERS sensors.

### 2.1. SERS mechanisms

To understand the mechanisms of SERS, it would be better to start with Raman scattering. In Raman scattering process, a molecule exposed to an oscillating electric field from incident light undergoes an induced polarizability with the dipole moment  $P_0$  and emits scattered light at a frequency shifted by

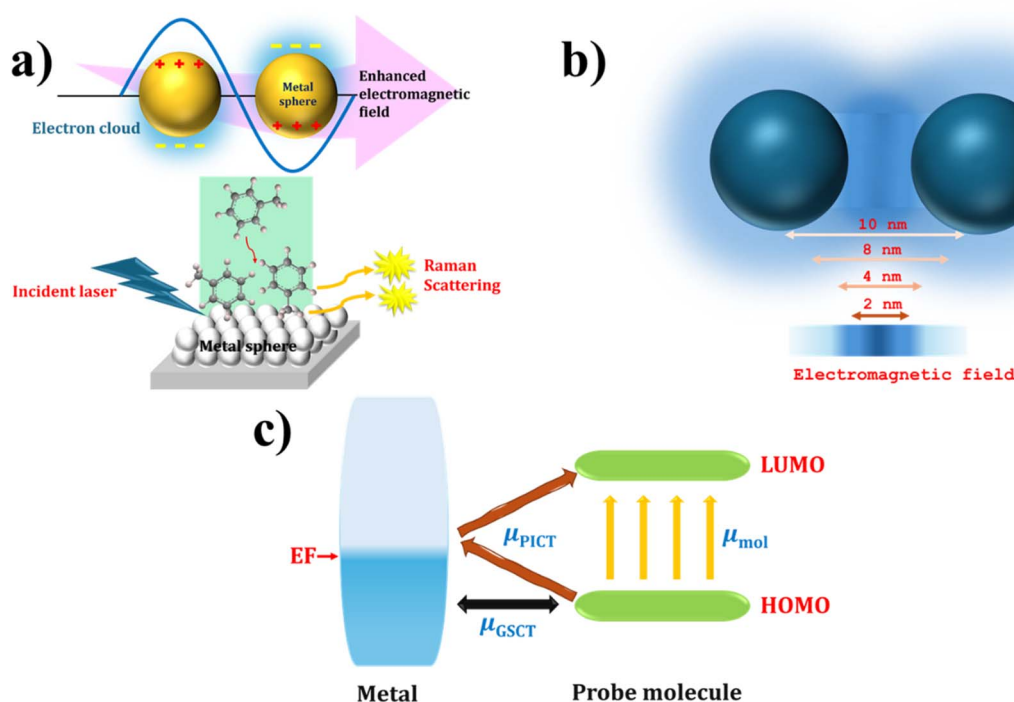


Fig. 1 Schematic illustration of (a) localized surface plasmon resonance and SERS effect *via* electromagnetic mechanism; (b) hot spots within small interparticle distance; (c) chemical enhancements in SERS.



its vibrational modes (Raman shift) with a frequency of  $\omega_R$ .<sup>29,30</sup> The magnitude of  $P_0$  depends on the change in polarizability ( $\alpha_0^R$ ) of electron during molecular vibration and the intensity of the incident electromagnetic radiation ( $E_0$ ) with a frequency of  $\omega_0$ . This can be described as equation below:

$$P_0(\omega_0) = \alpha_0^R(\omega_0, \omega_R) \times E_0(\omega_0) \quad (1)$$

In simple terms, the Raman scattering process requires the interaction of two main elements to occur: a molecule and an incident radiation. For that molecule to experience SERS effect, another element must be involved: a metal nanostructure, usually noble metal. Noble metals are rich in free electrons. Thus, when excited by an incident light, its conductive electrons undergo collective oscillations, generating an electromagnetic field around the dielectric and metal interface (Fig. 1b). If the frequency of the incident light  $\omega_0$  is resonant with that of the electron oscillation, surface plasmon resonance (SPR) is triggered. Thanks to the nanoscale dimensions of the metallic particles, the oscillation is confined, which is referred as localized surface plasmon resonance (LSPR).<sup>31</sup> Ding *et al.* described the enhancement of electromagnetic field as a two-step process.<sup>32</sup> First, thanks to the LSPR, the local electromagnetic field ( $E_{Loc}$ ) around the metallic NPs is enhanced at the incident frequency ( $\omega_0$ ). The SERS enhancement factor is proportional to the square of  $E_{Loc}$  at  $\omega_0$  as follows:

$$G_1(\omega_0) = [E_{Loc}(\omega_0)/E_0(\omega_0)]^2 \quad (2)$$

Second, at the scattered frequency ( $\omega_R$ ), strong mutual coupling occurs between the induced dipole of the molecule and the oscillating dipoles of the plasmonic nanoparticles (NPs), further enhancing the scattered Raman signal. It is resonant Raman scattering. Similar to the first step, the SERS enhancement factor in the second step is proportional to the square of  $E_{Loc}$  at  $\omega_R$  (eqn (3)).

$$G_2(\omega_R) = [E_{Loc}(\omega_R)/E_0(\omega_R)]^2 \quad (3)$$

For analytes with low vibrational frequencies, the enhancement factors of the two steps can be considered as comparable ( $G_1(\omega_0) \approx G_2(\omega_0)$ ). Thus, the SERS enhancement factor is about proportional to the fourth power of  $E_{Loc}$ .

$$G = G_1(\omega_0) G_2(\omega_0) \approx [E_{Loc}(\omega_0)/E_0(\omega_0)]^4 \quad (4)$$

Importantly, the electromagnetic field is not distributed uniformly around metallic nanostructures. As mentioned above, the confinement of electron oscillation triggers LSPR. Thus, narrow regions on those nanostructures such as edges, tips, corners, *etc.* are highly localized. Besides, interparticle nanogaps are convenient for resonant Raman scattering, leading to local field enhancement (Fig. 1a). Regions where the electromagnetic field is intensely amplified due to strong LSPR are called SERS hot spots. Scaling with the fourth power (eqn (4)), a small enhancement in the local field could lead to an

enormous change in SERS enhancement. It is the main principle of electromagnetic mechanism (EM) in SERS.

While EM is responsible for the change of the value  $E_0$  in eqn (1), chemical mechanism (CM) can lead to the modification of the value  $\alpha_0^R$ . The change in polarizability of the analytes in SERS effect requires the adsorptions of those molecules onto the surface of the metallic nanostructures. The changes in  $\alpha_0^R$  could be due to either chemical complexation or charge transfer (CT).<sup>33–36</sup> Chemical complexation is the formation of a complex between an analyte and a nanostructure *via* chemisorption. This interaction alters the polarizability, orientation and symmetry of the molecule relative to its unbound state, thereby activating certain vibrational modes. However, Moskovits claimed that complex formation could not contribute significant enhancements to  $\alpha_0^R$  unless the metal–ligand bond introduced CT transitions.<sup>34</sup> These processes can alter electron density distribution within organic molecules, resulting in increased polarizability and subsequently enhancing the Raman scattering response. CT can occur in either non-resonant or resonant pathways but they all involve the electronic coupling between the analyte molecules and the metallic nanostructures (Fig. 1c).<sup>35,36</sup> The non-resonant one does not require any excitation. It arises when chemical bonds are created between the analytes and the SERS substrate, which is called interfacial ground-state charge transfer (GSCT). In contrast, photo-induced charge transfer (PICT) involves photo-excitation, which generates energetic (“hot”) electrons to be exchanged between the Fermi level of metals and the highest occupied orbital (HOMO) or the lowest unoccupied molecular orbital (LUMO) levels of the analytes. Besides, CT resonance or resonance Raman scattering (RRS) occurs when the frequency of the excitation laser is close to the electronic transition of the analyte molecules, leading to electronic excitation within those molecules, resulting in resonance Raman effect, which enhances Raman scattering. Fluorescent molecules are more prone to undergoing this CT pathway.

The explanation of eqn (1) shows that both EM and CM contribute to SERS enhancements. Thus, the Raman dipole moment in SERS effect can be defined as:

$$P(\omega_R) = \alpha^R(\omega_0, \omega_R) \times E_{Loc}(\omega_0) \quad (5)$$

in which  $\alpha^R$  is the altered Raman polarization under SERS condition and  $E_{Loc}$  is the enhanced electromagnetic field around the metallic nanostructures. However, the contributions of two mechanisms are not comparable. While EM has been reported to contribute up to  $10^{11}$  to SERS enhancements, the contribution of CM is less than  $10^3$ .<sup>37</sup>

## 2.2. Key factors to improve SERS sensing performance

Understanding about the mechanisms of SERS allows researchers to optimize the performance of SERS sensing systems. In this section, we discuss the key factors to boost SERS sensing performance including sensitivity, selectivity, uniformity and practicability and briefly highlight several strategies that have been developed to address each of these aspects. In



the following section, selected strategies will be discussed in detail (Fig. 2).

**2.2.1. Sensitivity.** In general, SERS sensing performance highly depends on EM and CM as these enhancements significantly amplify the Raman signal, enabling the detection of analytes at extremely low concentrations and thereby determining the overall sensitivity of the sensor. Both CM and EM enhancement requires the adsorption of analytes onto metallic nanostructures. In CM enhancement, the interaction between substrate and the adsorbed molecules is necessary for the CT processes, which lead to changes in polarizability of the molecules. In EM enhancement, the analyte molecules could only experience the local magnetic field if they are located near the surface of the metallic nanostructures. Many analytes can be adsorbed directly into the surface of the metallic nanostructures. Molecules containing functional groups such as –SH, –NH<sub>2</sub> and –COOH can bind to the metallic surface and replace capping agents.<sup>48,49</sup> However, not all analytes possess such functional groups, which limits their ability to adsorb effectively onto the metallic surface of the SERS substrates. Thus, several strategies have been developed to improve the adsorption rate. For example, nanostructures surfaces can be functionalized with a layer of chemical compound that can immobilize the desired analytes *via* electrostatic repulsion,<sup>50</sup> hydrogen bond,<sup>51</sup> or covalent bond<sup>52</sup> to enhance the binding

affinity. Another approach is modifying the SERS substrate for better adsorption capacity. Instead of using only metallic NPs, researchers designed and developed nanocomposite materials by incorporating metallic NPs with other components, such as graphene oxide (GO)<sup>53,54</sup> and metal–organic frameworks (MOFs).<sup>55,56</sup> The adsorption of analytes onto those non-metallic components in the nanocomposite not only positions the molecules near the LSPR-active metallic sites to benefit from EM enhancement, but also improves CT processes in the cases the analytes are adsorbed onto the semiconductor in metal–semiconductor nanocomposites, leading to better SERS enhancements.<sup>57,58</sup>

Regarding the enormous contribution of EM to total SERS enhancements, creating hot spots for SERS enhancements is another key factor to improve SERS signal. Metallic nanostructures with sharp tips, corners, edges have been designed and developed as SERS active substrates.<sup>59–61</sup> In another approach, SERS enhancements could also originate from the plasmon formed at the small gaps between NPs (usually <10 nm), with an enhancement factor up to 10<sup>12</sup>.<sup>62</sup> Thus, other groups fabricated dimer or trimer nanostructures to trap the analytes in the hot spots between NPs for significant enhancements in SERS signal.<sup>63,64</sup> Besides, metallic nanoparticles could also be grafted onto 3-dimensional (3D) scaffold to create numerous interparticle nanogaps around the scaffold.<sup>65,66</sup> Although smaller interparticle gaps could lead to more intensely amplified electromagnetic field, it is worth mentioning that once the gap size reaches sub-nanometre scale, quantum effects would be introduced between the NPs and suppress SERS effects.<sup>32</sup>

**2.2.2. Selectivity.** SERS has the ability to identify analytes through their “fingerprint” spectra, however, in complex mixtures, multiple compounds can be adsorbed onto or near the SERS-active surface and experience the SERS effects, leading to interference. Moreover, biological samples usually contain various molecules, which could be similar in structure. For example, in plants, salicylic acid and methylbenzoate are two members of benzenoid class with similar structural features. As a result, their vibration spectra can have overlapping peaks, which makes it difficult to distinguish them. Thus, the intrinsic selectivity of SERS is not sufficient in complex samples. To improve the selectivity of the SERS sensors, it is necessary to functionalize with specific molecules to capture the desired analytes. This strategy also helps improve the CT processes as discussed in the last section. However, it requires more specific interactions, such as biological recognition<sup>67,68</sup> and chemical derivatization,<sup>69,70</sup> for the best selectivity.

**2.2.3. Uniformity.** Since the electromagnetic field is unevenly distributed around metallic nanostructures, uniformity has been always a challenge for SERS sensors. The electromagnetic field is amplified at the hot spots, such as edges, tips, corners, *etc.* of the NPs as well as the interparticle nanogaps. Therefore, the SERS signal of a sample is mainly contributed by the molecules located on/into those hot spots. If the interaction between the NPs and the analytes is weak, they can move around or diffuse into and out of the interparticle gaps (between the NPs), leading to the fluctuation of SERS



Fig. 2 Several main factors and strategies to improve SERS sensing performance. Illustration reproduced from ref. 38 with permission from the PCCP owner societies, copyright 2015; ref. 39 with permission from Springer Nature, copyright 2017; ref. 40 with permission from MPDI, copyright 2023; ref. 41 with permission from MPDI, copyright 2022; ref. 42 with permission from Elsevier, copyright 2019; ref. 43 with permission from MPDI, copyright 2021; ref. 44 with permission from The Royal Society of Chemistry copyright 2023; ref. 45 with permission from MPDI, copyright 2022; ref. 46 with permission Springer Nature, copyright 2017; ref. 47 with permission from The American Chemical Society, copyright 2015.



signals. Once again, it emphasizes the importance of NP functionalization. Besides, well-controlled nanostructured materials could be fabricated to improve the uniformity of SERS substrates. Researchers have prepared colloids with well-defined morphologies, size distribution and good dispersity thanks to the assistance of coating agents such as citrate,<sup>71</sup> cetyltrimethylammonium bromide (CTAB),<sup>72</sup> and polyvinylpyrrolidone (PVP)<sup>73</sup> and employed them as building blocks to fabricate SERS substrates. NPs were reported to self-assemble on solid supports, leading to relatively uniform SERS substrates.<sup>74</sup> In another approach, the assembly of NPs can be directed by polymers, allowing the control of NP spacing.<sup>75,76</sup> However, researchers could take it to another level by preparing NPs by lithography method, resulting in highly uniform substrates.<sup>77,78</sup>

**2.2.4. Practicability.** Despite being a powerful analytical tool, most SERS measurements have been performed in the laboratory. Translating SERS into practical applications with real samples is still challenging because of its scalability, production cost and ease of use. To improve the practicability of SERS, researchers need to overcome those barriers, allowing the applications of SERS to be widespread, especially in plant health monitoring. With the use of noble metal nanoparticles, SERS substrates were expected to be expensive, especially when fabricated using sophisticated techniques such as electron beam lithography. However, there are other methods of synthesizing which are more cost-effective such as chemical, and especially electrochemical synthesis, allowing gold and silver colloids to be produced at large volumes and low cost. More economic approaches such as self-assembly and inkjet printing can be employed to create SERS-active surfaces with reduced production costs. Additionally, the integration of polymers as flexible supports or structural scaffolds has shown promise in improving both the uniformity and scalability of SERS substrates. For example, incorporating nanoparticles into polymer films,<sup>79,80</sup> tapes,<sup>81</sup> or paper-based materials<sup>82,83</sup> allows for affordable sensing platforms. The use of these flexible substrates also simplifies sample collection and preparation, which is suitable for field-based or point-of-care applications. Besides, nanocomposites in which metallic NPs are embedded in matrices such as GO,<sup>83</sup> MOFs,<sup>84</sup> or semiconductors<sup>85</sup> are promising options for scalable and cost-effective production while simultaneously enhancing SERS efficiency.

Furthermore, functionalization of SERS substrates with specific binding agents allows the sensors to detect the desired analytes even in complex real samples. It reduces complex sample processing, allowing untrained people to perform the measurements in field-based conditions.

Reviewing several key factors boosting SERS sensing performance and some strategies employed to enhance them reveals that certain approaches can simultaneously improve multiple aspects. For example, the functionalization of nanoparticles not only enhances signal intensity but also contributes to greater selectivity and practical applicability. Meanwhile, some strategies come with the trade-offs. For instance, while sophisticated fabrication techniques such as lithography offer superior uniformity in SERS substrates, they also significantly

increase production costs, potentially limiting scalability. Therefore, researchers must carefully weigh these considerations and tailor their strategies to suit the specific requirements of each application.

In the next section, we focus on several main strategies which are suitable to elevate the multiple factors and contribute to significant improvement in overall SERS sensing performance with examples of recent established reports. These include: (i) generating hot spots to amplify EM enhancements; (ii) designing and developing nanocomposites to improve adsorption of analytes, therefore, elevating CT processes; (iii) functionalizing NPs to boost selectivity, molecular adsorption and practicability; (iv) fabricating flexible SERS substrates suitable for real-life applications while controlling NP assembly to achieve improved uniformity (Fig. 2). While the examples reviewed may not be directly related to plant health monitoring, all demonstrate the application of SERS sensors in plant-based matrices.

### 3. Strategies to enhance SERS sensing performance

#### 3.1. Hot spots formation *via* material designing

**3.1.1. Shape controlled NPs.** EM enhancement in SERS is strongly influenced by shape, size and compositions of nanoparticles. The “lightning rod effect” refers to the strong localization and amplification of electromagnetic field at sharp tips or edges of metallic nanostructures, which is similar to how lightning is attracted to the tip of a metal rod. As a result, anisotropic NPs such as nanorods, nanostars, nanoprisms and nanocubes, exhibits significant EM enhancements compared to nanospheres. Haes *et al.* employed discrete dipole approximation numerical method to estimate the maximized values of local electric field at the surface of three different shapes of NPs (*i.e.*, a sphere, a cube and a pyramid) to be on the order of  $\sim 10^2$ ,  $\sim 10^3$ , and  $\sim 10^4$ , respectively, based on the LSPR peak of each.<sup>86</sup>

While nanospheres usually exhibit a single, symmetrical SPR corresponding to uniform electron oscillations in all directions, anisotropic NPs show multiple SPR modes, such as transverse and longitudinal modes in nanorods and tip-localized modes in nanostars.<sup>87,88</sup> Thus, selecting the wavelength of excitation light for SERS using spherical NPs is simpler. Once the excitation wavelength closely matches the SPR band of the NPs, localized surface plasmons are resonantly excited, leading to the best SERS enhancement.<sup>89</sup> Meanwhile, anisotropic shapes drive it more complicated. For example, nanorods have two SPR bands, *i.e.*, transverse and longitudinal. The longitudinal mode (along the long axis of the nanorods), which is usually detected at the longer wavelengths, is more polarization-sensitive.<sup>90</sup> Thus, the longitudinal one is more relevant for SERS excitation. Moreover, it is highly tunable. Orendorff *et al.* reported that adjusting the length and width of the nanorods could allow the longitudinal SPR mode of Au nanorods to tune from about 650 nm to more than 1200 nm when the aspect ratio (length/width) increased from 2 to 16. The author also observed similar trends in silver nanorods. When the aspect ratio increased from 3.5 to 10, the



longitudinal SPR mode was shifted from about 535 nm to about 615 nm.<sup>91</sup> Therefore, the aspect ratio can be adjusted to achieve suitable SPR bands for maximal SERS enhancements.

In designing SERS nanoprobe, precision in the placement of Raman reporter molecules is paramount, particularly given the greater heterogeneity in EM field distributions. It is crucial to ensure that these reporter molecules are strategically positioned within the zones of amplified EM fields to optimize the SERS effect. Orendorff *et al.* compared SERS enhancements of Au and Ag nanorods with different aspects of ratio and Au and Ag spheres (aspect ratio = 1). Under the excitation at 633 nm, Ag nanorod with aspect ratio of 10 and Au nanorod with aspect ratio of 1.7 exhibited 10–10<sup>2</sup> greater SERS enhancements than others using 4-mecartopyridine (4-MTP), 4-aminothophenol (4-ATP) and 2,2'-bipyridine as analytes.<sup>91</sup>

NPs with more sharp tips such as nanostars were fabricated to concentrate intense electromagnetic fields around their tips, leading to significant enhancements in SERS signal. A well-known method to prepare Au nanostar is using Ag<sup>+</sup> as a shape-directing agent. Ag<sup>+</sup> can selectively adsorb on certain facet of preformed Au seeds, suppressing the growth at those sites and promoting the formation of anisotropic Au nanostructures.<sup>92</sup> Besides, many other methods can be used to synthesis Au and Ag nanostars. For example, Au nanostars have also been fabricated thanks to the assistance of Good's buffer as well as PVP in DMF solvent.<sup>93</sup> Ag nanostars were reported to be prepared using microwave heating of AgNO<sub>3</sub> and trisodium citrate.<sup>94</sup> The outstanding SERS enhancements of nanostars were also proved in experimental studies. For instance, Oliveira *et al.* compared the enhancement factors (EFs) of Ag nanospheres and nanostars and reported EFs ranging of 10<sup>6</sup>–10<sup>7</sup>

using Ag nanostars while Ag nanospheres showed one order of magnitude lower in EF under identical conditions.<sup>95</sup>

However, the fact that the electromagnetic field concentrates at the tips of the material also emphasizes the heterogeneity of its distribution in the surface of anisotropic NPs, which is obviously the main drawback of this approach. The advantages and disadvantages of each approach are listed in Table 1.

**3.1.2. Intergap nanoparticles.** Nanogaps created between two or more NPs act as highly efficient hot spots, offering much stronger SERS signal enhancement than a single, isolated one. Dimeric, trimeric and even tetrameric nanostructures have been designed and developed and employed as active SERS substrates. Schuknecht *et al.* designed tip-to-tip Au nanorods using DNA origami scaffold with controlled gaps of around 8 nm, which could accommodate proteins like streptavidin and thrombin.<sup>63</sup> The sensing systems exhibited impressive sensitivity of single-protein detection within sub-second integration time. However, the fabrication of this sensor required complex DNA-origami designing, which is costly and potentially unstable in biological environments. In a recent study, Ignatane *et al.* developed another method to synthesize dimeric AuNPs. AuNPs with a diameter of around 60 nm were placed within dumbbell-shaped pits etched *via* focused ion beam lithography on glass substrates *via* capillary force-assisted dip-coating, ensuring precise dimer positioning and controlled spacing. The gap of 12 nm led to an enhancement factor of 2.9 × 10<sup>5</sup> when detecting Rhodamine B.<sup>96</sup> Obviously, this approach allowed reliable control over interparticle spacing thanks to the geometry of the pits. However, some pits only partially filled with NPs, affecting the uniformity. Moreover, focused ion beam lithography is slow and expensive for large area patterning.

**Table 1** Advantages and disadvantages of several common strategies to create SER hot spots

Strategies		Advantages	Disadvantages
Nanoparticle shapes	Isotropic	- Simple preparation - Relatively high structural uniformity - Cost-effective	Relatively low SERS enhancement
	Anisotropic	- High tunability - High EM enhancement	- Complex preparation - Low signal uniformity
Internanogap	DNA assisted assembly	- High EM enhancement	- Complex preparation - Low synthetic yield - Light orientation angle dependence - Expensive - Unstable in biological environment
	Lithography assisted assembly	- High EM enhancement	- Complex preparation - Low synthetic yield -Light orientation angle dependence -Expensive
	Self-assembly	- High EM enhancement - Simple preparation - Cost-effective	- Low synthetic yield - Light orientation angle dependence - Low uniformity due to gap variation
	Core-shell configuration	- High EM enhancement  - High tunability ( <i>i.e.</i> , size, density, material of satellites)	- Complexed EM enhancement mechanism among the core and the satellites - Low uniformity (but better than other intragap creating approaches)
Intrananogap	- High EM enhancement  - Highly robust SERS signal	- Complex preparation - Low synthetic yield - Expensive	



Compared to those approaches, self-assembly of NPs is simpler. Arbuz *et al.* controlled the formation of AuNP dimers and trimers *via* mixed self-assembled monolayers (mixed SAMs) of mercaptocarboxylic acids on 100-nm AuNPs, achieving nanogaps from 0.8 nm to 2.3 nm.<sup>97</sup> When using the dimeric structures with the gap of around 1.0 nm to detect R6G, the EF value was 4–5 folds higher than that obtained with the use of monomers. However, it was difficult to control gap sizes, therefore, the gap variation could lead to variation in EF. In case using anisotropic NPs as monomers, random orientation of the dimers when on substrates might reduce the uniformity of the sensor.

Using similar approaches, trimeric and tetrameric NPs have been fabricated and employed as SERS substrates.<sup>97–99</sup> It has been reported that trimers outperformed dimers and tetramers outperformed trimers due to multiple gap junctions and Fano-like plasmon modes, leading to stronger plasmonic coupling.<sup>100</sup>

Another approach, which could be considered as a branch of intergap nanoparticle configuration, is core–satellite arrangement. This configuration involves multiple satellite nanoparticles arranged around a central core, greatly enhancing the local electromagnetic field, particularly at the junctions between the core and satellites or between adjacent satellites.<sup>101,102</sup> Unlike dimers and trimers, which have a specific orientation in space, core–satellite structures are more symmetric and uniform in all directions, ensuring that a consistent electromagnetic field can be created. Thus, it is expected to generate reproducible SERS signal. Tang *et al.* reported on the fabrication of Au core–satellite nanostructures consisting of an Au core (120–140 nm in diameter) decorated with smaller Au satellite NPs (20–40 nm) *via* 1,8-octanedithiol (C8DT) linkers. The assembly can be performed rapidly in around 30 min with controlled ionic strength to regulate satellite coverage and gap width (2–3 nm). Analytes such as *p*-ATP can be adsorbed into the gaps and detected *via* SERS measurements.<sup>103</sup> Although the fabrication of this core–satellite configuration was simple, the assembly of satellites around the core could not be well-controlled. Thus, variability in gap size and satellite coverage can lead to EF heterogeneity.

**3.1.3. Intragap nanoparticles.** In addition to intergap NP creation, researchers also engineered nanogaps within a single NP, forming what is known as an intra-nanogap structures. These structures offer superior mechanical stability and structural integrity, resulting in strong, consistent, and quantifiable SERS signals that are less sensitive to external variations. For example, Nam's group invented Au-nanogapped nanoparticle (Au-NNP) structures.<sup>104</sup> Gold cores with diameter of 12–20 nm are coated with thiolated DNA or polymer spacer. Subsequently, a secondary Au shell was grown around this layer, forming a well-defined nanogap of 1 nm, resulting in an EF of about  $1 \times 10^8$  to  $5 \times 10^9$ , allowing single molecule detection. However, the functionalization of NPs with DNA or polymer spacer must be precise and growth of the shell must be well-controlled. Once the gap is too thin, it may induce quantum tunneling and reduce EF. Moreover, it is not flexible for capturing analytes externally. In another approach, Kim *et al.* prepared dealloyed intra-nanogap particles using Au/Ag alloy NPs are etched so that

only Ag dissolved, forming a hollow porous Au shell around a core with internal gaps between the core and the cell, allowing analyte to be adsorbed into the gap. When used as DNA detection probes, these structures enable ultra-sensitive detection down to 10 aM with EF of  $1.1 \times 10^8$ .<sup>105</sup> However, the fabrication requires complex dealloying process, and controlling precise gap dimensions is technically challenging. Cheng *et al.* fabricated gap-enhanced Au nanodumbbells. Starting with an Au nanorod with a length of around 10 nm, the authors selectively grow a gold shell at each tip in the presence of CTAB, forming tip-coated shells separated by a 1-nm nanogap containing a monolayer of 4-nitrobenzenethiol (4-NBT) as a Raman reporter. Compared to the initial Au nanorod, SERS intensity of 4-NBT increased by 100 times. EF was calculated to be  $10^7$ – $10^8$ .<sup>106</sup> However, this anisotropic shape introduce polarization sensitivity to the sensing systems. Moreover, it is complex to control the growth of the tip-shell.

Shape, gap, and how you control both are the levers that set the electromagnetic game. Anisotropic particles (rods, stars, prisms, cubes) concentrate fields at tips/edges (“lightning-rod” effect) and add tunable plasmon modes, so matching the excitation to the dominant mode (often the longitudinal resonance) delivers large EM gains, but also spatial heterogeneity across a single particle. Interparticle gaps push enhancement further: dimers/trimers and core–satellite assemblies create junction hot spots whose strength scales as the gap narrows into the 1–3 nm regime, yet reproducibility hinges on how precisely those gaps and orientations are set (DNA/origami, templated pits, or controlled self-assembly beat stochastic clustering). Intragap designs build the junction inside one particle (gap-shells, nanodumbbells, dealloyed hollow shells), stabilizing the hot spot against handling and drift and enabling quantifiable signals; the trade-offs are synthetic complexity, shell-growth control, and the tunneling ceiling as gaps approach ~1 nm. Across these families, the same rules dominate: tune resonance to the measurement band, confine and standardize the gap architecture, and pair the geometry with disciplined readout (internal-standard ratios, fixed sampling optics). The result is the practical sweet spot, apparent EF in the  $10^6$ – $10^9$  band with single- to low-tens-percent precision when geometry is patterned or internally template.<sup>107–109</sup> The main remaining limit of hotspot stochasticity which increase variance unless geometry are controlled, which would be discussed in Section 5.

### 3.2. Nanocomposites fabrication

While EM dominates most noble metal-based SERS substrates, boosting CT is essential for improving sensitivity toward analytes with low Raman cross-sections or weak binding affinities. This has driven the development of nanocomposites that integrate plasmonic metals with semiconductors, metal–organic frameworks (MOFs) or graphene oxide (GO) which offer tailored interfaces and electronic structures conducive to CT-driven SERS enhancement.

**3.2.1. Metal–semiconductor nanocomposites.** While noble metals, such as Au, Ag, offer intense LSPR that amplified



electromagnetic field, they usually exhibit limited interaction with adsorbed molecules in the ground state. In general, most adsorbate molecules are held to the metallic surface *via* physisorption. Only molecules containing specific functional groups, such as thiol, carboxyl and primary amine, could be adsorbed onto the metallic surface *via* chemical interactions. It constrains their ability to enhance Raman signal of analytes *via* CT processes. In contrast, semiconductors promote the adsorption of analytes onto SERS substrate as they are richer surface chemistry with possible presence of hydroxyl groups as well as metal–oxide bonds. As a result, their surface charge and polarity are adjustable, which is beneficial for the adsorption of various analytes.<sup>110</sup> Moreover, abundant surface defects on the surface of semiconductors can improve analyte adsorption on vacancy-rich surfaces.<sup>111–113</sup> Furthermore, some semiconductors were reported to provide specific binding sites for analytes.<sup>114</sup> In addition, they introduce new energy levels and interfacial pathways that promote efficient electron exchange with the analyte, thereby significantly boosting SERS signals *via* CM.<sup>115,116</sup> The fact that more analyte molecules are adsorbed onto the surface of semiconductors in nanocomposite materials also allow them to experience EM enhancement from the plasmonic materials.

In metal–semiconductor nanocomposite-based SERS sensing systems, CT processes follow two principal pathways: (i) semiconductor-to-metal-to-analyte and (ii) metal-to-semiconductor-to-analyte. These routes arise from the complex band alignment and interfacial energetics between the metals, the semiconductors, and the analytes.

In the semiconductor-to-metal-to-analyte pathway, photoexcitation of the semiconductor generates electron–hole pairs. Under ultraviolet, certain semiconductors, such as TiO<sub>2</sub>, WO<sub>3</sub>, WS<sub>2</sub>, *etc.*, undergo photoinduced defect engineering, in which UV excitation can cause cooperative oxygen removal, leading to the formation of surface oxygen vacancies of line defects.<sup>36</sup> These vacancies introduce new donor states within the bandgap, typically just below the conduction band (CB) of the semiconductor. These defect states act as electron reservoirs for CT process to send hot electrons to adsorbed analytes. Only UV sources with sufficient photon energy could generate the electron–hole pairs. Almohammed *et al.* proposed that the energy of the incident photons had to be greater than or equal to the bandgap energy of the semiconductor. This band gap is varied among semiconductors. For example, the band gap of anatase TiO<sub>2</sub> is around 3.2 eV while this value of WO<sub>3</sub> is approximately 2.6 eV.<sup>117</sup> Once the oxygen vacancy states are formed, the photoexcited electrons can be trapped in these mid-gap defect states. These trapped electrons are then available to be injected to the Fermi level of the metal.<sup>117</sup> As a result, the density of hot electrons on the surface of the metal increases, allowing more electrons to go into CT processes, leading to CM enhancement in SERS effect. It is called photo-induced enhanced Raman spectroscopy (PIERS). This mechanism in oxygen-deficient TiO<sub>2</sub>/Ag has helped enhance SERS signal of urea, a low Raman cross-section molecule. SERS intensity of urea on TiO<sub>2</sub>/Ag was up to 7.45 times higher than that on AgNPs.<sup>118</sup> In another study, Glass *et al.* compared PIERS effects of three types of oxide

thin films, including TiO<sub>2</sub>, WO<sub>3</sub> and ZnO coated with AuNPs using a reporter molecule (4-mercaptobenzoic acid – 4-MBA). The results showed that all three metal–semiconductor nanocomposite expressed PIERS effect. WO<sub>3</sub> films exhibited strongest enhancement rates and slower vacancy healing than TiO<sub>2</sub> or ZnO. ZnO formed oxygen vacancies under UV, but these vacancies are less stable in air and recombine quickly, thus, ZnO/Ag composite showed the worst SERS performance compared to the other two.<sup>119</sup> Similar enhancements were also achieved in other metal–semiconductor nanocomposites such as Au@WS<sub>2</sub> (ref. 120) and AuNPs-diphenylalanine peptide nanotubes.<sup>121</sup>

On the other hand, the metal-to-semiconductor-to-analyte pathway originates from the excitation of surface plasmons in noble metal nanoparticles, which produce hot electrons. These hot electrons can be injected to coupled semiconductor *via* Schottky barrier.<sup>36,122,123</sup> Then, these excited electrons would be transferred to analytes *via* the chemical bonding between them and the semiconductor.<sup>122,123</sup> As mentioned above, in comparison to TiO<sub>2</sub> and WO<sub>3</sub>, ZnO is less effective for PIERS-based SERS applications. Nevertheless, ZnO remains widely studied as a component of metal–semiconductor SERS nanocomposites, not for its PIERS activity, but because of its performance in this CT pathway. Zhou *et al.* fabricated Au–ZnO nanorods as SERS substrates for dopamine detection. Plasmon-induced charge transfer (PICT) occurred, allowing hot electrons to be transferred from Au to ZnO after the excitation by a laser source, followed by ground-state charge transfer (GSCT) from ZnO to dopamine *via* chemical bond between them. As a result, the SERS signal of dopamine on Au–ZnO nanorods were double that on AuNPs.<sup>123</sup> Similarly, the integration with MnO<sub>2</sub> nanosheet improved SERS signal of tricyclazole (TCZ), compared to the use of AgNPs. This allowed the MnO<sub>2</sub>/Ag-based SERS sensors to detect TCZ at concentrations down to  $6.0 \times 10^{-12}$  M in standard solutions and  $1.0 \times 10^{-11}$  M in rice samples.<sup>85</sup>

**3.2.2. Metal-MOF nanocomposite materials.** MOFs integrated with plasmonic nano materials play a multifaceted role in enhancing the performance of SERS substrates by enabling selective analyte adsorption, facilitating interfacial CT and improving substrate stability and uniformity. First, MOFs act as molecular sieves and pre-concentrators thanks to their well-defined pore structures and tunable surface chemistry. Zeolitic Imidazolate Framework-8 (ZIF-8), a common-used MOF have been employed to encapsulate AuNPs in a 2021 study to detect volatile organic compound (VOCs) such as toluene and ethylbenzene.<sup>124</sup> The porous structure helped ZIF-8 to selectively allow small molecules to diffuse through and approach the Au core, improving both selectivity and SERS signal. In a more recent study, Ag/ZIF-8 also promoted selectivity of SERS-based sensors in aqueous environments, in which urea could be detected in the interferences of larger organic compounds.<sup>84</sup> In both studies, the selective adsorption mechanism ensured that the analytes were precisely positioned within the electromagnetic (EM) hot spots, significantly boosting sensitivity. Second, MOF can directly contribute to chemical CT process with analyte. For example, Shao *et al.* designed a SERS substrate consisting of AgNPs embedded within a MIL-101(Cr) thin film.<sup>125</sup> In



this system, in addition to the EM enhancement from AgNPs, CrO<sub>3</sub> metal clusters with the MOF structures generated CT interaction with 4-ATP, resulting in an impressive limit of detection (LOD) of 10<sup>-11</sup> M for 4-ATP and 10<sup>-7</sup> M for nitrofurantoin while the RSD is only, representing high uniformity of the sensors. Finally, MOFs improve physical stability of the nanocomposite materials, prevent metallic materials from aggregation. Tran *et al.* reported on integrating amino-functionalized MOF-5 film with AgNPs to fabricate SERS substrates, which maintained over 70% of initial signal intensity even after 120 days of storage, with LOD of 1.78 × 10<sup>-10</sup> M and 1.26 × 10<sup>-12</sup> M for methylene blue (MB) and RhB, respectively.<sup>126</sup>

**3.2.3. Other nanocomposite materials.** Other materials such as polymer and carbon-based nanomaterials could also be integrated to produce nanocomposite SERS substrates. For example, Pan *et al.* fabricated AgNPs coated with poly(3,4-ethylenedioxythiophene) polystyrene sulfonate (PEDOT:PSS), using 4-MBA as the probe molecule. The increase in  $b_2/a_1$  band intensity ratios of 4-MBA and calculation of degree of CT ( $\rho_{CT}$ ) exhibited that the polymer actively contributes to CM *via* CT transitions. The author also optimized the thickness of the polymer coat. At the concentration of 0.8% PEDOT:PSS, the sensing system achieved the maximum SERS intensity and the highest  $\rho_{CT}$  of 0.65.<sup>127</sup> In addition, carbon-based nanomaterials, particularly graphene oxide (GO) and reduced graphene oxide (rGO), can also be integrated with metallic NPs to improve SERS enhancement. In a study on Ag-GO nanocomposites, Kasztelan *et al.* claimed that CM enhancement arises through CT between GO and analyte molecules adsorbed on the substrate.<sup>128</sup> In another study, AgNPs grown on rGO sheets was utilized as SERS substrates to detect 4-aminophenol and fenvalerate (a pesticide) at concentrations as low as 10<sup>-10</sup> M and 1.69 × 10<sup>-9</sup> M, respectively. In this composite material, rGO acted as a scaffold to capture and enrich analyte *via*  $\pi$ - $\pi$  interaction, bringing them nearer to AgNPs to experience EM enhancement. Moreover, it promoted CT between the SERS substrates and the analytes.<sup>129</sup>

Integrating plasmonic metals with semiconductors, MOFs, or conductive carbons systematically adds CT channels and tailored adsorption to the baseline EM gain, which is exactly what low-cross-section or weakly adsorbing analytes need. In metal-semiconductor hybrids, CT arises either from vacancy-mediated, UV-driven PIERS (semiconductor-to-metal-to-analyte) or from plasmon-generated carriers injected across the Schottky contact (metal-to-semiconductor-to-analyte), with defect density, band alignment, and illumination wavelength governing the payoff. Metal-MOF architectures contribute by molecular sieving and pre-concentration at hot spots, orientation control at functional nodes/linkers, and, when redox-active centers are present, direct CT with the analyte; MOF shells also temper aggregation/aging if thickness is kept within the near-field decay length. Polymer and carbon composites (*e.g.*, PEDOT:PSS coats; GO/rGO scaffolds) supply  $\pi$ - $\pi$  or electrostatic capture and additional CT pathways while improving mechanical robustness. Across these families, reports commonly land in the apparent EF of about 10<sup>5</sup>-10<sup>8</sup> and LOD high-pM to low-

nM bands when chemistry is matched to the target;<sup>130</sup> precision improves on patterned/ordered supports. Recurrent limits are batch variability in interfacial states (defects, linker thickness), spectral overlap from organic shells, diffusion/kinetic bottlenecks in thick MOF layers, and photo/chemical drift (vacancy healing, polymer background). The practical fix is to couple these materials choices to the operating discipline detailed later, including stable reporter/internal standard schemes, matrix-matched calibration, and explicit precision tiers, so CT benefits translate into reproducible, decision-grade sensing rather than one-off boosts.

### 3.3. Nanoparticle functionalization

SERS achieving high sensitivity and selectivity heavily depends on the interaction between analyte molecules and the nanostructured substrate surface. A key strategy to enhance the SERS signal involves functionalizing the substrate with ligands that can attract, retain, and orient analyte molecules precisely within electromagnetic hot spots, allowing them to experience EM and CM enhancements from the active substrates. Several surface functionalization strategies have been developed to improve molecular affinity, reduce signal fluctuation, and enhance the signal-to-noise ratio in SERS based on different interaction between functional groups of the ligands and the analytes.

**3.3.1. Electrostatic functionalization.** Electrostatic interaction is a simple but effective strategy. NPs capped with coating agents such as citrate (negatively charged) or CTAB (positively charged) can selectively attract opposite charged analytes.<sup>131,132</sup> Ranishenka *et al.* reported on the functionalization of AgNPs using both a negatively charged thiol, *i.e.*, mercaptopropionic acid, and positively charged ones, *i.e.*, 2-dimethylaminoethanethiol, thiocholine to detect two porphyrins: CuTMpyP<sub>4</sub> (cationic) and CuTSPP<sub>4</sub> (anionic). The result showed that AgNPs capped with negative thiol exhibited strong SERS enhancement for the cationic CuTMpyP<sub>4</sub> and no signal enhancement for the anionic CuTSPP<sub>4</sub>. In contrast, SERS signal of CuTSPP<sub>4</sub> could be observed on AgNPs capped with positive thiol while CuTMpyP<sub>4</sub> could not.<sup>132</sup>

**3.3.2. Host-guest recognition.** In host-guest chemistry, NPs are functionalized with molecular host such as cyclodextrins, cucurbit[*n*]urils, and calix[*n*]arenes.<sup>133-135</sup> These molecules have internal hydrophobic cavities that can accommodate guest molecules through non-covalent interactions like hydrogen bonding, hydrophobic forces, and  $\pi$ - $\pi$  stacking. Functionalized host molecules with thiol or other anchoring groups can attach to the metal surface, positioning the analyte closely to the metallic NPs. This approach provides high affinity and selectivity for various small analytes, such as aromatic hydrocarbons and pesticides, and can also assist in nanoparticle assembly. For example, AuNPs were assembled on silica then functionalized with thiol linked  $\beta$ -CD dimers to achieve  $\beta$ -CD dimer@Ag@SiO<sub>2</sub> core-shell nanostructures. Perylene, a polycyclic aromatic hydrocarbon, is a planar aromatic compound, which could form inclusion complexes with the hydrophobic cavity of  $\beta$ -CD dimer. Therefore, functionalizing with  $\beta$ -CD dimer allowed perylene to be close to Ag surface, experiencing



SERS enhancement. As a result, the sensitivity of the  $\beta$ -CD dimer@Ag@SiO<sub>2</sub> is 1000 times higher than Ag@SiO<sub>2</sub> without functionalization, allowing perylene to be detected at concentrations as low as 10<sup>-8</sup> M.<sup>133</sup> Similarly, cucurbit[7]uril (CB[7]) was grafted onto AuNPs as a host for creatinine, resulting in an LOD of 12.5 ng mL<sup>-1</sup>.<sup>134</sup>

**3.3.3. Biological recognition.** Biomolecules such as single-stranded DNA, antibodies, aptamers offer high specificity to the SERS sensors once they are employed to functionalize NPs. These biorecognition elements can selectively bind analytes ranging from small molecules to proteins and cells. For example, Yang *et al.* functionalize both ends of Au nanorods with capture and detection protein against prostate-specific antigen (PSA), forming end-to-end assemblies *via* antigen-mediated crosslinking.<sup>136</sup> PSA binds to the antibodies on separate Au nanorods causing a chain-like assembly with uniform gaps of around 5.6 nm, generating SERS hot spots. As a result, the intensity of SERS reporter malachite green isothiocyanate (MGITC) was proportional to the concentration of PSA in diluted human serum.

**3.3.4. Molecular imprinting.** Molecular imprinting polymers (MIPs) are fabricated by polymerizing monomers in the presence of a target molecule. This molecule is then removed to create complementary binding sites. When NPs coated with MIPs can adsorb analytes with high selectivity. For example, a MIP was synthesized using melamine, methacrylic acid as the functional monomer, and ethylene glycol dimethacrylate as cross-linker. It was used in conjugation with Ag dendrite nanostructures to fabricate SERS substrate to detect melamine in whole milk samples, resulting in an LOD of about 12  $\mu$ M.<sup>137</sup> This steric recognition method mimics biological systems while maintaining robustness. Besides, molecular imprinting layers can enforce selectivity and resist nonspecific adsorption in colored extracts; recent work introduced an “inspector” recognition mechanism on imprinted polydopamine (PDA) over SERS tags that achieves absolute enantiomeric discrimination.<sup>138</sup>

**3.3.5. Chemical derivatization.** In this strategy, NPs are coated with reagents that chemically react with target analytes,

forming SERS active products. This formation is reflected in SERS spectra. For example, Ag nanostructures functionalized with 4-ATP that contains amine group (-NH<sub>2</sub>) to form imine (N=CH-) with aldehyde analytes, which is called Schiff-base formation. The formation alters both molecular vibrational modes and plasmonic CT behavior of the coating agents. The SERS spectra of 4-ATP, especially *b*<sub>2</sub> vibration, change in intensity and position upon the binding of aldehyde analytes. Sinha *et al.* employed this principle to develop SERS sensors for formaldehyde, acetaldehyde and benzaldehyde with LODs of about 1  $\mu$ M.<sup>139</sup> Besides, boronate affinity is applied to detect diol-containing molecules, such as dopamine and glucose. For example, Choi *et al.* developed a dopamine SERS sensor using AgNPs coated with 4-mercaptophenylboronic acid (4-MPBA). The boronic acid selectively interacted with dopamine *via* boronate ester formation with its diol groups. It led to the shift from 1076 cm<sup>-1</sup> to 1084 cm<sup>-1</sup> in the SERS spectra in the increase of dopamine concentration.<sup>140</sup>

Surface chemistry is the lever that turns adsorption into analysis. Electrostatic capping (*e.g.*, citrate, CTAB, charged thiols) and host-guest receptors (cyclodextrins, cucurbiturils, calixarenes) pre-concentrate small molecules at hot spots; biorecognition (aptamers, antibodies, DNA probes) enforces lock-and-key selectivity; molecular imprinting supplies shape-complementary binding on robust polymer shells; and derivatization (*e.g.*, boronate esters, Schiff bases, reporter coupling) converts weak or Raman-silent targets into SERS-active species. Across recent methodological surveys, such reporter-/receptor-assisted formats typically deliver apparent EF of about 10<sup>5</sup>-10<sup>8</sup> with single- to low-tens-percent reproducibility when geometry and preprocessing are controlled.<sup>141</sup> Principal failure modes are band overlap between reporter and analyte, competitive adsorption in plant/water matrices, and fluorescence-sensitive baselines; these are mitigated by ratiometric readout (stable internal standard or label-free calibrant), minimal-chemistry cleanup, and explicit reporting of preprocessing parameters. Advantages and trade-offs for each route are summarized in Table 2.

Table 2 Advantages and disadvantages of NP functionalization strategies

Strategy	Mechanism	Advantages	Disadvantages
Electrostatic interaction	Coulombic attraction between charged ligand and analyte	- Simple to implement - Fast adsorption - Applicable to ionic analytes	- Limited selectivity - Sensitive to pH and ionic strength - Weak binding
Host-guest inclusion complexes	Molecular encapsulation <i>via</i> macrocyclic hosts	- High specificity for hydrophobic/aromatic targets - Orientation control	- Limited to guest-compatible molecules - Possible steric hindrance
Biological recognition (aptamers/antibodies)	Specific molecular recognition (lock-and-key)	- Extremely high specificity - Ideal for biomolecules	- Costly - Sensitive to denaturation and storage
Molecular imprinting (MIP)	Shape and functional group complementarity	- Low detection limits - High selectivity - Reusable - Stable under harsh conditions	- Limited to aqueous systems - Complex synthesis - Possible template leakage - Slower binding kinetics
Chemical derivatization	Covalent or reactive bonding to analyte ( <i>e.g.</i> , Schiff base)	- Converts non-SERS-active targets - Enhances selectivity and signal	- Requires specific reactive groups - May alter target structure or activity



### 3.4. Flexible substrates

Flexible SERS substrates have emerged as promising tools for rapid, sensitive, and portable molecular detection, which is promising to real-world applications. Unlike conventional rigid substrates (glass or silicon), flexible platforms made of paper, polymers, films, or textiles offer mechanical adaptability, cost-effectiveness, and suitability for on-site applications. Flexible SERS substrates rely on plasmonic nanostructures anchored to bendable platforms such as paper, polydimethylsiloxane (PDMS), poly(tetrafluoroethylene) (PTFE), adhesive tape, cotton, or chitosan sponge. These materials are chosen for their flexibility, availability, and compatibility with low-cost processing.<sup>142–144</sup> Flexible SERS substrates can be fabricated through several scalable and effective methods. One common approach is *in situ* nanoparticle growth, where metal precursors are chemically reduced directly onto the surface of a flexible substrate such as cotton or chitosan, forming Ag or AuNPs for immediate SERS activation.<sup>145,146</sup> Another widely used technique is dip-coating or soaking, where the substrate is immersed in a colloidal suspension of plasmonic nanoparticles, allowing uniform adsorption across the surface. Paper and cellulose filter are suitable for this fabrication as they are hydrophilic but not dissolve in water.<sup>82</sup> Other materials such as GO can be integrated to improve the binding of NPs onto the paper substrates.<sup>83</sup> More advanced methods like printing and lithography, including inkjet printing and nanoimprint techniques, enable the creation of patterned or large-area SERS films with high reproducibility and design control. In addition to paper and PDMS, AgNPs have been printed onto polyethylene naphthalate (PEN), commercial overhead projector (OHP) and polyethylene terephthalate (PET) film to fabricate flexible substrates for *trans*-1,2-bis(4-pyridyl)ethylene (BPY), steric acid and

melamine, respectively.<sup>147–149</sup> Additionally, encapsulation techniques involve sandwiching plasmonic nanostructures between protective polymer layers, which enhances mechanical durability while preserving the flexibility of the sensor.<sup>150,151</sup> Table 3 shows the comparisons of the fabrication methods with their advantages and limitations. These fabrication strategies support the mass production of flexible, reproducible, and low-cost SERS substrates suitable for disposable or wearable applications. These features make flexible SERS ideal for real-time, *in situ* sensing in non-laboratory environments.

Flexible SERS platforms translate plasmonic enhancement onto bendable, low-cost supports (paper, PDMS, PTFE, tapes, textiles, chitosan), enabling on-site sampling and large-area coverage with simple handling. Scalable routes, such as *in situ* growth of Ag/Au on fibrous matrices, dip/soak loading of colloids onto hydrophilic cellulose, and printing/nanoimprint patterning on PEN/OHP/PET, provide tunable hotspot density and meter-scale throughput while staying compatible with disposable formats. Across recent studies, reported reproducibility for flexible substrates typically falls in the single- to low-tens-percent RSD range, with lower values on patterned paper/printed films and higher values on unconstrained foams; when authors separate precision levels, spot/position RSDs are commonly around 4–16%, device-to-device comparisons about 6–22%, and, where available, across-run values up to ~25%.<sup>81,146,152–154</sup>

## 4. Applications of SERS for plant health and crop quality monitoring

Fig. 3 demonstrates the integration of the SERS technique across all phases of precision agriculture, encompassing the

Table 3 Advantages and disadvantages of several SERS flexible substrate fabrication methods

Fabrication method	Flexible substrate examples	Advantages	Disadvantages
<i>In situ</i> nanoparticle growth	Cotton, chitosan sponge, textile paper	<ul style="list-style-type: none"> <li>- Strong NP-substrate bonding enhances durability</li> <li>- Uniform coating on fibrous/porous surfaces</li> <li>- Simple, low-cost chemical reduction process</li> </ul>	<ul style="list-style-type: none"> <li>- Less control over NP size/shape and interparticle gap</li> <li>- Hotspot density may vary batch-to-batch</li> </ul>
Dip-coating/soaking	Paper, cotton fabric, cellulose filter, textile fibers	<ul style="list-style-type: none"> <li>- Simple and scalable</li> <li>- Compatible with various colloidal NP systems</li> <li>- Substrate retains porosity and flexibility</li> </ul>	<ul style="list-style-type: none"> <li>- Weak NP adhesion unless further modified, therefore lower mechanical durability</li> </ul>
Printing and lithography	Paper, PDMS, PET film	<ul style="list-style-type: none"> <li>- High reproducibility and design control</li> <li>- Scalable for large-area or patterned substrates</li> <li>- Suitable for integrated or multiplexed sensors</li> </ul>	<ul style="list-style-type: none"> <li>- Requires advanced tools (<i>e.g.</i>, inkjet/screen printers or molds)</li> </ul>
Encapsulation	PDMS, PMMA, PU film, adhesive film	<ul style="list-style-type: none"> <li>- Excellent mechanical durability</li> <li>- Protects plasmonic surface from oxidation, abrasion, or humidity</li> <li>- Long-term signal retention</li> </ul>	<ul style="list-style-type: none"> <li>- More expensive than dip-coating or <i>in situ</i> growth</li> <li>- Signal attenuation if polymer layer too thick</li> <li>- More complex fabrication (multi-step embedding or transfer)</li> </ul>



pre-cultivation stage (e.g., soil and water quality assessment), the cultivation phase (e.g., monitoring of plant stress and nutrient levels, detection of pathogen infection, *etc.*) and the pre-harvest period (e.g., evaluation of crop maturity, detection of pathogens and pesticide residue level). The figure also outlines key target analytes for SERS based detection throughout the three cultivation stages, including plant stress biomarkers (e.g., VOCs, phytohormones, reactive oxygen species, and plant metabolites), nutrients, environment contaminants (e.g., heavy metal ions, pesticide residues, and engineered NPs), as well as pathogens.

#### 4.1. Plant stress biomarkers

Plants constantly interact with their surrounding environment, and any changes, whether caused by drought, salinity, pathogen invasion, or mechanical injury, can trigger the production of specific chemical signatures known as stress markers. Among them, volatile organic compounds (VOCs) serve as rapid airborne signals for intra- and interplant communication, phytohormones act as central regulators of stress signaling pathways, ROS function as both damaging agents and key secondary messengers, and secondary metabolites contribute to defense and adaptation mechanisms. The timely detection of these markers not only enables early stress diagnosis but also offers valuable insights into the underlying physiological and biochemical processes. In the following sections, we discuss recent progress in SERS-based approaches for monitoring each

category of plant stress markers, highlighting unique sensing strategies and their relevance to plant health monitoring, which is also summarized in Table 4.

**4.1.1. Volatile organic compounds.** Volatile organic compounds (VOCs) play a critical role in plant physiology, acting as chemical signals for inter- and intra-species communication and as defense agents against biotic and abiotic stress. These compounds, including alkanes, alkenes, alcohols, aldehydes, esters, and carboxylic acids, are emitted from nearly all plant organs such as leaves, fruit, flowers and roots, primarily through stomatal openings.<sup>162,163</sup> For examples, leave usually emit methanol and isoprenoids while fruit release aroma-related alcohol and esters.<sup>164</sup> In addition, at different developmental stages, metabolic stages and when exposure to external stimuli such as pathogens or environment stressors, plants release distinct types of VOCs at various concentrations.<sup>164,165</sup> Since VOCs profiles shift dynamically in response to physiological changes, VOCs can be significant signals for noninvasive assessment of plant health.<sup>166</sup>

Conventional VOC detection techniques such as GC-MS and proton transfer reaction mass spectrometry (PTR-MS) offer high sensitivity and chemical specificity but are limited by their high cost, lack of portability, and inability to perform real-time, on-site measurements.<sup>165</sup> In this context, SERS has recently gained attention as a powerful and ultrasensitive technique for VOC detection. Its ability to generate distinct molecular fingerprints with high sensitivity allows it to be suitable for *in*

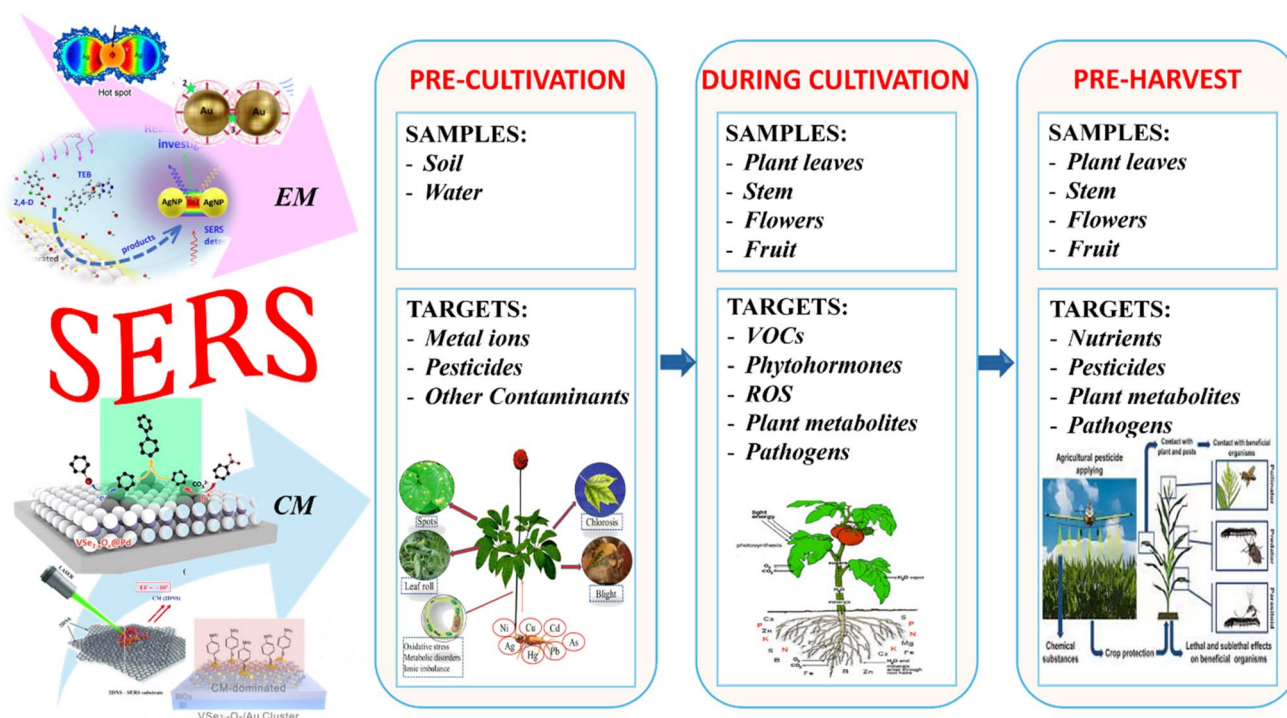


Fig. 3 SERS in different stages of cultivation. Illustration reproduce from ref. 40 with permission from MDPI, copyright 2023; ref. 155 with permission from The Royal Society of Chemistry, copyright 2014; ref. 156 with permission from Elsevier, copyright 2023; ref. 157 with permission from Elsevier, copyright 2023; ref. 158 with permission from The American Chemistry Society, copyright 2023; ref. 159 with permission from American Chemistry Society, copyright 2023; ref. 160 with permission from Nature Springer, copyright 2015; and ref. 161 with permission from Nature Springer, copyright 2022.





Table 4 Several SERS-based sensors for plant stress markers

Analytes	SERS substrate	Strategy	Real sample/context	LOD	Ref.
<b>VOCS</b> Various VOCs ((E)-2-hexenal, (Z)-3-hexenyl acetate, caryophyllene, and others) Methyl salicylate (MeSA)	Polymer layer with Ag nanospheres  4-MPBA-functionalized AuNPs	Adsorptive polymer collect and pre-concentrate VOCs on flexible substrate  4-MPBA can form a reversible cyclic boronate ester with the ortho-hydroxyl group of MeSA Adsorptive MOF	Caterpillar-induced cotton plants and healthy ones (headspace) Lab MeSA vapor model	— 0.608 ppb	80 167
Formaldehyde, benzaldehyde, oxalaldehyde, glutaraldehyde, salicylaldehyde and 4-nitrobenzaldehyde Plant VOCs (infection, interplant communication)	AgNPs@ZIP-8  Ag nanoshells coated with polymers (AgNS@PDDA, AgNS@PVA, AgNS@PAA) are infiltrated into plant leaf tissues	Each polymer has different chemical affinities for specific VOCs: PDDA (cationic) – negatively charged or polar VOCs PAA (anionic) – hydrogen bond donors; PVA (neutral, hydrophilic) – alcohols and esters	Fungi-infected strawberry plants <i>in situ</i>	—	168
<b>Phytohormones</b> Salicylic acid	Ag colloids activated by $\text{Ca}^{2+}/\text{Pb}^{2+}/\text{Al}^{3+}$	$\text{Ca}^{2+}/\text{Pb}^{2+}/\text{Al}^{3+}$ adions create CT interactions with SA adsorbed on Ag Ehrlich reaction derivatization	Plant tissue (mung bean, pea, soybean, black bean sprouts) Wheat leaves	50 $\mu\text{M}$ 2.0 nM 0.67 fM	181 69 68
Indole-3-butyric acid (IBA)	AuNPs	Aptamer-based competitive binding with SERS report Reaction between NO and OPD	Endogenous NO in living macrophages	10–7 M	170
ABA	Aptamer grafted $\text{Fe}_3\text{O}_4$ magnetic NPs + Au@Ag nanosphere with 4-MBA <i>o</i> -Phenylenediamine modified AuNPs	—	Plant-extract demo Grape skin	—	171 172
<b>Stress-related secondary metabolites</b> Anthocyanins Anthocyanins	AgNPs $\text{TiO}_2$ nanotube films decorated with AgNPs $\text{Cu}_2\text{O}$ -Ag SERS substrate	Exciting at anthocyanin absorption for resonance Uniform array	Plant extracts ( <i>Stevia rebaudiana</i> leaves, coffee beans, <i>Lonicera japonica</i> leaves, and <i>Eucommia ulmoides</i> flowers)	10–350 $\mu\text{M}$	173
Chlorogenic acid					
<b>ROS</b> $\text{H}_2\text{O}_2$	Ag decahedral NPs functionalized with 4-MPBA	Boronic acid $\rightarrow$ phenol reaction	Tobacco leaves	0.5 $\mu\text{M}$	70

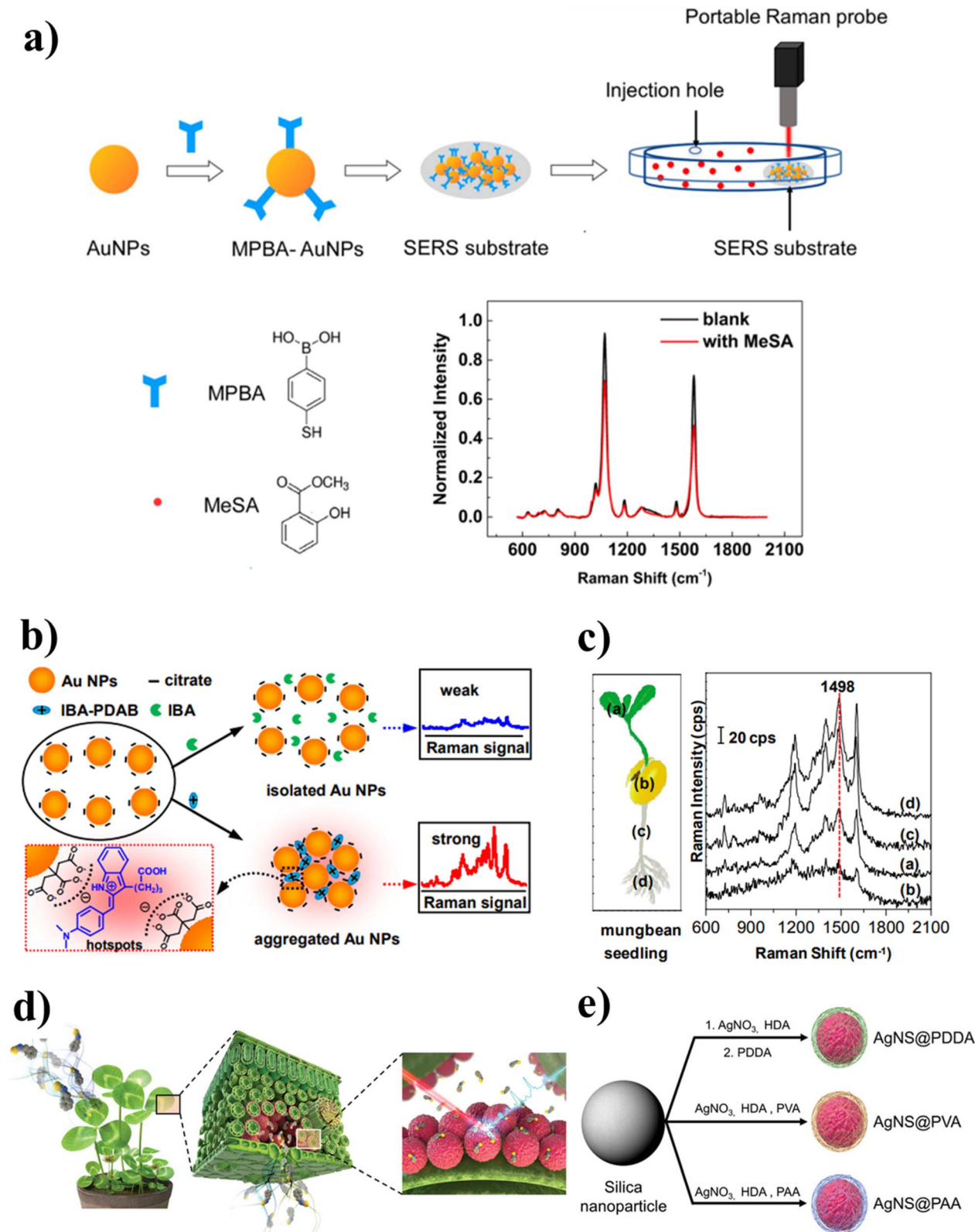


Fig. 4 Several SERS sensing systems to detect plant stress markers. (a) Capped AuNPs with 4-MPBA to detect MeSA, adapted from ref. 167 with permission from The American Chemical Society, copyright 2022; (b) detection of IBA using PDAB to create hot spots among AuNPs, adapted from ref. 69 with permission from The American Chemical Society, copyright 2017; (c) comparisons of IBA concentrations in root, stem, hypocotyl and leaf of mungbean seedling, adapted from ref. 69 with permission from The American Chemical Society, copyright 2017; (d) and (e) nanobionic plant sensors by infiltrating polymer-coated silver nanoshells (AgNS@PDDA/PVA/PAA) directly into leaf tissues, adapted from ref. 168 with permission from John Wiley & Son, Inc., copyright 2025.



*situ* monitoring of plants VOCs under natural growth conditions. The main challenge to detect VOCs in plants is the adsorption of the analytes in their gas phase onto SERS substrates. Several research groups have functionalized NPs to effectively capture the desired VOCs. For example, Song *et al.* capped AuNPs with 4-MPBA, which can form a reversible cyclic boronate ester with the ortho-hydroxyl groups of methyl salicylate (MeSA), a volatile biomarker released by plant under stress (Fig. 4a).<sup>167</sup> As a result, MeSA could be detected at concentrations down to 0.686 ppb. In a recent study, Choi *et al.* developed a nanobionic plant sensor by infiltrating polymer-coated silver nanoshells (AgNS@PDDA/PVA/PAA) directly into leaf tissues (Fig. 4d), enabling *in vivo* SERS detection of VOCs at parts-per-trillion levels. Each polymer provided distinct chemical affinity: PDDA (poly(diallyldimethylammonium chloride), cationic) targeted negatively charged or polar VOCs, PAA (poly(acrylic acid), anionic) interacted with hydrogen bond donors, and PVA (poly(vinyl alcohol), neutral, hydrophilic) captured alcohols and esters (Fig. 4e). The embedded nanosensors localized near stomata, allowing spatially resolved, real-time VOC mapping without harming plant physiology, and were successfully applied for multiplex VOC monitoring and early detection of pathogen-induced plant signals in the field.<sup>168</sup> Besides, high adsorptive SERS substrates were also designed with the integration of MOF and polymer. Park *et al.* designed a sensing substrate using adsorptive polymer to detect various VOCs in cotton plants, which allowed the authors to differentiate caterpillar-induced plants and healthy ones.<sup>80</sup>

**4.1.2. Phytohormones.** Phytohormones are vital chemical messengers produced in specific plant tissues that orchestrate a wide range of developmental and stress-related processes. These include classical hormones such as indole-3-acetic acid (IAA), cytokinins (CK), gibberellins (GA), abscisic acid (ABA), and ethylene, as well as recently recognized regulators including brassinosteroid (BRs), jasmonates (JA) and salicylic acid (SA).<sup>169</sup> Each hormone serves distinct role: IAA governs cell elongation and tissue differentiation, GA promotes stem growth, ABA mediates responses to abiotic stress through stomatal regulation, ethylene controls senescence and fruit ripening, SA and JA are central to plant immune signaling.<sup>169</sup> Given their low endogenous concentration and critical functional roles, sensitive and selective detection of phytohormones is essential for plant health monitoring. Thus, in many studies on employing SERS to detect phytohormones, researchers selected the strategies of NP functionalization. For example, the phytohormone indole-3-butyric acid (IBA), itself, is Raman-inactive and lacks resonance with typical Raman excitation wavelengths. Wang *et al.* used the Ehrlich reaction, reacting IBA with *p*-(dimethylamino)benzaldehyde (PDAB). This reaction forms a cationic derivative (IBA-PDAB) featuring an extended  $\pi$ -conjugated system, which introduces a new absorption band at around 626 nm, making it both Raman-active and resonant with excitation light. The cationic IBA-PDAB readily causes aggregation of negatively charged, citrate-stabilized gold nanoparticles (Au NPs). Aggregation clusters created SERS hotspots to amplify the Raman signal (Fig. 4b). The system achieved ultra-sensitive SERS detection with an LOD of about 2.0 nM. It

allowed them to compare IBA concentrations in different parts of mungbean, including root, hypocotyl, stem and leaf (Fig. 4c).<sup>69</sup> Nitric oxide could also be detected using a similar strategy as *o*-phenylenediamine (OPD) on AuNPs surface reacted with NO to produce a distinctive SERS fingerprint. It allowed NO to be detected at concentrations down to  $10^{-7}$  M. Even though, the real sample of the research is not plant-related, NO is a plant signaling molecule with hormone-like effects and sometimes referred to as a “gasotransmitter” in plant biology.<sup>170</sup> Zhang *et al.* selected a more complicated strategy to sense ABA. In their aptamer-based SERS sensor, capture probe comprised Fe<sub>3</sub>O<sub>4</sub> magnetic NPs linked to aptamer complements while SERS signal probes were Au@Ag nanospheres carrying 4-MBA as an internal standard. ABA binding triggered probe release, leading to a reproducible SERS signal decay. It resulted in an LOD of 0.67 fM.<sup>68</sup> Although highly sensitive and selective SERS sensors for phytohormones have been designed and developed, SERS-based sensing systems for many other phytohormones such as cytokinins, gibberellins, jasmonates, and ethylene, have not been fabricated. Thus, they are promising targets for future development of SERS sensors for plant health monitoring.

**4.1.3. Secondary metabolites.** Plant metabolites play critical roles in maintaining physiological functions and responding to environmental challenges. These metabolites are generally classified into primary metabolites, such as carbohydrates (*e.g.*, glucose, sucrose, fructose), which are essential for fundamental processes like growth and energy metabolism, and secondary metabolites, which include organic acids, alkaloids, phenolic compounds, and terpenoids. While primary metabolites are vital for development, secondary metabolites are often linked to the plant's defense mechanisms and are key indicators of abiotic and biotic stress responses. In this context, we only discuss SERS sensors developed to sense plant metabolites as stress markers. The others will be highlighted in another section about non-stress-related plant metabolites. Anthocyanins, pigments that accumulate in response to light stress, drought or pathogen attack, have been targeted by SERS in several studies with different substrates. In a 2015 study, Zaffino *et al.* employed simple Ag colloid as SERS substrates to sense anthocyanins in qualitative speciation.<sup>171</sup> More recently, Sarto *et al.* introduced an active substrate built from TiO<sub>2</sub> nanotube film decorated with AgNPs to determine anthocyanin in grape skin extracts. The authors selected the laser at the wavelength matching anthocyanin absorption to promote resonance Raman, one of CT pathways as discussed in Section 2.1, allowing the amplification of SERS signal.<sup>172</sup> Also using semiconductors to integrate with plasmonic NPs in the effort of improving SERS, Liu *et al.* fabricated Cu<sub>2</sub>O-Ag array *via in situ* growth method to detect chlorogenic acid in plant extracts, leading to an EF of  $1.27 \times 10^5$  and uniformity RSD of 5.27%.<sup>173</sup>

**4.1.4. Reactive oxygen species (ROS).** Reactive oxygen species (ROS) are essential signaling molecules that allow plants to respond rapidly to environmental changes. They participate in perceiving both abiotic and biotic stresses, integrating external cues, and triggering stress-responsive signaling networks that contribute to plant defense and resilience.<sup>174</sup> Among the various ROS, hydrogen peroxide (H<sub>2</sub>O<sub>2</sub>) is



particularly significant due to its relative stability, lower reactivity, and electrical neutrality compared with more transient species such as superoxide anion radicals ( $O_2^{\cdot-}$ ) and hydroxyl radicals ( $\cdot OH$ ).<sup>175</sup> The detection of  $H_2O_2$  using SERS technique has been studied for years. Many research groups have designed and developed SERS sensors for  $H_2O_2$  in living cells and tissue. However, most of them were carried out in mammal cells. However, their principles could be translatable to plant cells and plant tissues. The most used strategies to detect  $H_2O_2$  is functionalization the SERS substrates with boronic acids, which react selectively with  $H_2O_2$ , even in complex biological matrices. This allowed the detection of this ROS at nM levels.<sup>176–178</sup> Similarly, Tian *et al.* fabricated Ag decahedral NPs (AgDeNPs) as SERS substrates. The sharp corner of the NPs helped localize electromagnetic field, allowing EM enhancements in Raman signal of the analytes. AgDeNPs is coated with 4-MPBA. In the presence of  $H_2O_2$ , it reacted with 4-MPBA to become 4-mercaptophenol, which was reflected in the SERS bands (*i.e.*, loss of B–O vibration bands (around  $1070\text{ cm}^{-1}$ ) and appearance of aromatic ring stretch bands (about  $1580\text{ cm}^{-1}$ )). As a result,  $H_2O_2$  was detected at concentrations of  $0.5\text{ }\mu\text{M}$ . The SERS substrates were infiltrated into tobacco leaves, which were suffered from abiotic stress, such as wounding and salt stress, to induce endogenous  $H_2O_2$  generation. SERS spectra were recorded *in vivo* directly from the leaf surface at various time points to monitor dynamic  $H_2O_2$  changes.<sup>70</sup> In another strategy,  $H_2O_2$  can oxidize TMB, which is reflected in its SERS spectra, allowing the detection of this ROS. Wang *et al.* designed  $Fe_3O_4@Ag$  core–satellite NPs to sense TMB and oxidized TMB (oxTMB). The SERS signal of oxTMB (on the Ag surface) tracks intracellular  $H_2O_2$ , achieving a wide linear range of  $1\text{ fM}$ – $1\text{ mM}$ .<sup>179</sup>

SERS has matured from proof-of-concepts to targeted, matrix-aware sensing across the major biomarker classes that report plant stress in real time. For VOCs, capture-first designs (boronic acids, polymer affinity shells, MOF/polymer adsorbers, and in-leaf nanobionic probes) solve the gas-phase adsorption bottleneck and enable on-plant, spatiotemporal readout at sub-ppb to ppt levels while preserving physiology. For phytohormones, chemical derivatization (to render Raman-active or resonant), receptor-mediated capture (aptamers/antibodies), and internal-standard ratiometry drive from nM to sub-nM quantitation despite low basal abundance and structural similarity. For secondary metabolites, semiconductor–plasmonic heterostructures and resonance-matched excitation boost weak or colored analytes (*e.g.*, anthocyanins, phenolics) and support uniform mapping in extracts and tissues. For ROS, reaction-reporter schemes (boronic acids  $\rightarrow$  phenols; TMB/oxTMB pairs) translate short-lived oxidants into stable spectral signatures, enabling *in vivo* tracking of  $H_2O_2$  dynamics in wounded or salt-stressed leaves. Common limits, such as adsorption competition, fluorescence, and device-to-device variance, are addressed upstream by selective interfaces and downstream by ratiometry and matrix-matched calibration. Standard operating procedures and validation pathways are consolidated in Sections 5 and 6.

Table 5 SERS-based sensors non-stress-related plant metabolites

Analytes	SERS substrate	Strategy	Real sample/context	LOD	Ref.
Citrus flavonoids (14 kinds, including naringenin, hesperetin, tangeretin, nobilletin, <i>etc.</i> ) EGCG (catechin)	Ag dendrites (displacement-grown) used after TLC  $MnO_2@Ag$ aerogel	TLC-SERS (2D TLC separation, then SERS on Ag dendrites)	Fresh orange juice and orange peel extracts	$10\text{--}16.7\text{ }\mu\text{M}$ (compound-dependent)	187
Ascorbic acid (vitamin C)	$GeO_2@Fe_3O_4/Au$ NP nanozyme composite	Dual-mode SERS/colorimetry <i>via</i> nanozyme activity Smartphone-readable dual-mode (colorimetry + SERS of oxTMB probe inhibited by AA)	Tea leaves (evaluation of eight teas) Fruits, vitamin-C drinks, tablets	$1\text{ }\mu\text{M}$ $6.162 \times 10^{-13}\text{ M}$ (SERS mode)	185 186
Riboflavin ( $B_2$ ) & cyanocobalamin ( $B_{12}$ ) Capsaicin	Nanopatterned 2D gratings on fused silica with 40 nm Ag film Au nanorods with 4-ATP diazo-coupling to form SERS-active azo dye anchored to Au AuNPs on glass	Hot spots created by nanopatterning  Reaction-based SERS (diazotization)	Fortified cereal extract  Gutter-oil discrimination	—  $3.24 \times 10^{-12}\text{ M}$	183 184
Fructose and pectin		Direct SERS	Commercial apple juice and apple/pear pulp (no pretreatment)	—	182



## 4.2. Non-stress-related plant metabolites

In addition to their roles as indicators of plant stress, metabolites also occur in many forms that are unrelated to stress responses yet remain highly relevant for agricultural, nutritional, and industrial purposes. These include primary metabolites involved in fundamental metabolic pathways and secondary metabolites contributing to traits such as flavor, color, and nutritional value. Monitoring these metabolites can provide farmers with valuable insights into whether crops are developing properly and whether their quality meets desired standards. In this section, we focus on SERS-based approaches for detecting such non-stress-related metabolites in plants, highlighting their potential in quality assessment, compositional analysis, and value-added product development. Several SERS sensors for these metabolites as well as their sensing strategies are listed in Table 5.

Because the Raman spectra of organic compounds can serve as unique molecular fingerprints, researchers have applied a direct SERS approach using only Au nanoparticles deposited on glass to detect fructose and pectin in fruit juice and pulp.<sup>182</sup>

Although the method provided only qualitative identification, it successfully demonstrated the capability of SERS to sense plant metabolites within complex sample matrices. To improve sensitivity of SERS sensing system, Radu *et al.* designed and developed nanopatterned 2D gratings on fused silica with 40 nm Ag film to create hot spots on the SERS substrates to detect two vitamins, riboflavin (B<sub>2</sub>) and cyanocobalamin (B<sub>12</sub>).<sup>183</sup> In another approach, Au nanorods were functionalized with 4-ATP, which could react with amine group in capsaicin and form SERS-active azo dyes anchored to Au surface (Fig. 5a). It kept more capsaicin molecules close to the Au surface to experience SERS effects, resulting in an impressive LOD of  $3.24 \times 10^{-12}$  M.<sup>184</sup> Besides, dual-mode sensors were designed to detect epigallocatechin gallate (EGCG)<sup>185</sup> and vitamin C,<sup>186</sup> in which SERS substrates also acted as nanozymes in colorimetric reactions. Moreover, thin-layer chromatography (TLC) has been coupled with SERS as a hybrid approach where TLC separates compound in the mixture and SERS detect them directly on the TLC plate. This combination allowed Li *et al.* to determine 14 kinds of citrus flavonoids at concentrations down to 10–16.7  $\mu$ M for each compound.<sup>187</sup>

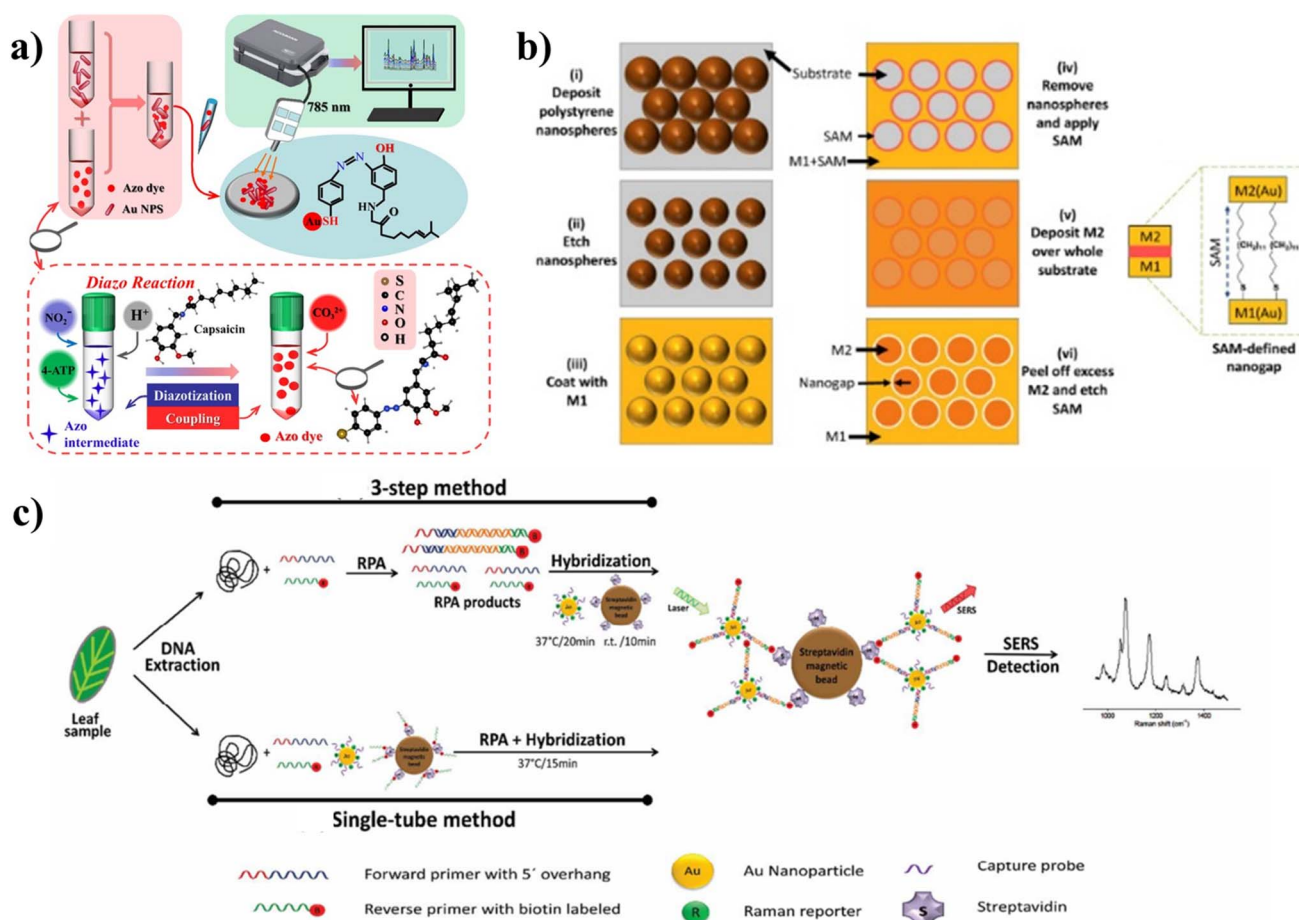


Fig. 5 (a) SERS sensor for capsaicin: Au nanorods with 4-ATP diazo-coupling to form SERS-active azo dye anchored to Au, reflected on SERS spectra, adapted from ref. 184 with permission from Nature Springer, copyright 2022; (b) combination of nanosphere lithography and adhesion lithography to prepare ring-shaped nanogaps for detection of nanoplastics, adapted from ref. 208 with permission from Frontier, copyright 2023; (c) schematic illustration of integrated recombinase polymerase amplification (RPA) with SERS nanotags for *Botrytis cinerea*, *P. syringae* and *Fusarium oxysporum*, adapted from ref. 215 with permission from The American Chemical Society, copyright 2016.



Beyond stress phenotyping, SERS is increasingly used for quality and compositional readouts in plants and plant-derived products. Three design logics recur. First, direct fingerprinting on simple Au/Ag supports can identify abundant targets in complex matrices (e.g., sugars, pectin), providing rapid screens when absolute sensitivity is secondary. Second, signal-engineering boosts weak analytes: nanopatterned films concentrate hot spots for vitamins; reactive capture/derivatization (e.g., 4-ATP to azo coupling with capsaicinoids) converts poorly scattering species into SERS-active products and drives LODs into the pM-to-fM regime; and dual-mode SERS-nanozyme assays add a colorimetric channel that co-validates SERS calls for polyphenols and antioxidants. Third, hybrid separations such as TLC-SERS physically resolve mixtures (flavonoids, phenolics) before readout, trading a minute of workflow for major gains in selectivity. Typical failure modes, including band overlap in polyphenol-rich extracts and matrix-driven adsorption bias, are mitigated by a short separation or derivatization step plus ratiometric readout and matrix-matched calibration (Section 5&6).

### 4.3. Contaminants

In precision agriculture, monitoring contaminants at different cultivation stages is key to maintaining an optimal growing environment. Pre-cultivation assessments of soil and irrigation water can identify harmful levels of heavy metals, pesticide residues, or engineered nanoparticles that may affect crop performance. During cultivation, targeted screening of plants for pesticides supports responsible use and integrated pest management. In the pre-harvest stage, rapid analysis of leaves, fruits, and flowers for pesticide residues, pathogens, and other contaminants provides real-time feedback on crop conditions. SERS offers a sensitive, rapid, and field-deployable tool for such multi-stage monitoring, enabling informed decisions throughout the production cycle. Table 6 summarizes several SERS-based sensors developed for detecting contaminants in soils, irrigation water, and plant tissues across different cultivation stages, highlighting the analytes, sensing strategies, substrates, and performance metrics.

**4.3.1. Heavy metal ions.** Monitoring heavy metal ions in soil and water prior to cultivation is essential for ensuring a safe and healthy growing environment, as excessive levels can hinder plant growth, reduce crop yields, and pose long-term environmental risks. Conventional *Anal. Methods*, such as inductively coupled plasma mass spectrometry (ICP-MS), optical emission spectroscopy (ICP-OES), atomic absorption spectroscopy (AAS), and anodic stripping voltammetry (ASV), offer high accuracy and trace-level quantification.<sup>188</sup> For example, ICP-MS is widely used for sensitive detection of metals in environmental samples due to its precision and multi-element capability.<sup>188</sup> However, these techniques typically demand extensive sample preparation, such as soil digestion or acidification, dedicated laboratory instrumentation, and skilled personnel, making them time-consuming and less suitable for *in situ* or rapid screening. In contrast, ASV, while offering portability and low-cost operation, involves electrodeposition steps and specialized electrodes, which is

traditionally mercury-based. This complicates field deployment and requires careful optimization.<sup>189</sup> SERS offers a powerful alternative, enabling rapid, sensitive, and on-site detection of heavy metal ions through their direct Raman signatures or *via* functionalized probes that selectively bind target ions. By integrating SERS into pre-cultivation soil and water management, farmers and agricultural managers can make informed decisions to prevent contamination-related losses and ensure sustainable cultivation practices.

Recent developments in SERS-based detection of heavy metal ions for pre-cultivation soil and water monitoring demonstrate both exceptional sensitivity and strong compliance with international regulatory thresholds, while highlighting clear differences between direct and indirect detection strategies. Direct SERS is less common but can be highly effective for certain species; for example, PVP-coated Ag nanocrystal arrays enable the direct adsorption of arsenate and arsenite oxyanions,<sup>190</sup> producing intrinsic Raman bands with an LOD of  $1 \mu\text{g L}^{-1}$  in real groundwater, which is well below the WHO drinking water limit ( $10 \mu\text{g L}^{-1}$ )<sup>191</sup> and the FAO irrigation threshold ( $100 \mu\text{g L}^{-1}$ ).<sup>192</sup> However, as most metal ions are weak Raman scatterers, indirect SERS is the predominant approach. This involves using selective ligands, chromogenic reagents, or biomolecular recognition elements that either form SERS-active complexes with the ion or modulate the signal of a pre-adsorbed Raman reporter. For example, Cr(VI) oxidation of diphenylcarbazide on MOF-Ag-TiO<sub>2</sub> substrates,<sup>193</sup> Cd<sup>2+</sup> chelation with alizarin and auxiliary ligands on AuNPs,<sup>194</sup> and Hg<sup>2+</sup> binding to 4-mercaptopyridine-functionalized Fe<sub>3</sub>O<sub>4</sub>@SiO<sub>2</sub>@Au magnetic NPs<sup>195</sup> resulted in LODs of  $0.26 \mu\text{g L}^{-1}$ ,  $0.01 \mu\text{g L}^{-1}$  and  $1 \mu\text{g L}^{-1}$ , respectively. In another study, Pb<sup>2+</sup> quantification with DNAzyme-activated polyA-Ag-AuNP chips achieves ultratrace detection with an LOD of  $1.84 \text{ ng L}^{-1}$ .<sup>196</sup> For soil extracts, Zn<sup>2+</sup> detection *via* Zn-4-(2-pyridylazo) resorcinol (Zn-PAR) complexation on Ag colloids allows qualitative speciation.<sup>197</sup> Table 6 also presents the linear range of each sensor as well as compares its LOD and range with official regulatory thresholds.

**4.3.2. Pesticides.** The intensive application of pesticides remains a common practice in agriculture to protect crops from pests and diseases. However, excessive or improper use can lead to residues that exceed maximum residue limits (MRLs), posing risks not only to consumer health but also to environmental sustainability and crop quality. Effective control of pesticide use during cultivation requires timely and reliable detection methods that can be deployed in the field to guide dosage adjustments and determine the appropriate harvest time. Traditional laboratory-based techniques, while accurate, are often time-consuming and require complex sample preparation, making them less suitable for rapid, on-site decision-making.<sup>198,199</sup> By enabling rapid pre-harvest testing, SERS-based sensors can help farmers ensure that pesticide residues remain within regulatory limits, reduce unnecessary chemical inputs, and support precision agriculture practices. The following section highlights recent advances in SERS-based detection of pesticides during cultivation, focusing on systems designed for in-field monitoring and early-stage intervention. Several SERS





Table 6 SERS-based sensors for contaminants in agricultural water, soil and plants

Analytes	SERS substrate	Strategy	Real sample	LOD/range	Permissible limit <sup>191,192</sup>	Ref.
<b>Heavy metal ions</b>						
As(v)/As(III)	PVP-coated Ag nanocrystal arrays	Direct SERS	Groundwater (real samples, standard-addition)	1 $\mu\text{g L}^{-1}$ ; linear 1–180 $\mu\text{g L}^{-1}$	10 $\mu\text{g L}^{-1}$ (WHO drinking water); 100 $\mu\text{g L}^{-1}$ (FAO irrigation water)	190
Cr(vi)	UiO-66 MOF/Ag/TiO <sub>2</sub>	Cr(vi) oxidizes diphenylcarbazide to SERS-active product	Lake water (spiked)	0.26 $\mu\text{g L}^{-1}$ (5 nM) in standards; 26 $\mu\text{g L}^{-1}$ (0.5 $\mu\text{M}$ ) in lake water	50 $\mu\text{g L}^{-1}$ (WHO total cr); 100 $\mu\text{g L}^{-1}$ (FAO irrigation water)	193
Cd(II)	AuNPs functionalized with alizarin + MPA/PDCA	Chelation changes reporter signal	Drinking water	0.01 $\mu\text{g L}^{-1}$ (10 ppt)	3 $\mu\text{g L}^{-1}$ (WHO drinking water); 10 $\mu\text{g L}^{-1}$ (FAO irrigation water)	194
Hg(II)	Fe <sub>3</sub> O <sub>4</sub> @SiO <sub>2</sub> @Au magnetic core-shell NPs	Coordination to reporter alters Raman signature	Environmental water	1 $\mu\text{g L}^{-1}$ –10 $\text{mg L}^{-1}$	6 $\mu\text{g L}^{-1}$ (WHO drinking water); ≤10 $\mu\text{g L}^{-1}$ (FAO irrigation water)	195
Zn(II)	Ag colloid + PAR chelation	Indirect SERS – Zn-PAR complex gives strong SERS fingerprint	Contaminated soil extracts	Qualitative ID; ~390 $\text{mg kg}^{-1}$ (UV-vis quant.)	3 $\text{mg L}^{-1}$ (WHO drinking water); 2 $\text{mg L}^{-1}$ (FAO irrigation water); 100–300 $\text{mg kg}^{-1}$ (soil guideline)	197
Pb(II)	DNAzyme/polyA-Ag-Au NP chip	Indirect SERS – Pb <sup>2+</sup> triggers DNAzyme cleavage altering reporter proximity	Lake, tap, industrial wastewater	1.84 $\text{ng L}^{-1}$ (8.9 pM)	10 $\mu\text{g L}^{-1}$ (WHO drinking water); 5 $\mu\text{g L}^{-1}$ (FAO irrigation water)	196
<b>Pesticides</b>						
Flumetsulam	AuNP colloid	NaCl and MgSO <sub>4</sub> induced aggregation to create hot spots	Wheat (extract)	0.01 $\text{mg kg}^{-1}$ ; linear 0.05–5 $\text{mg kg}^{-1}$ (in-matrix)	0.05 $\text{mg kg}^{-1}$ (China GB 2763 wheat MRL)	204
Pymetrozine	Au@AgNP	Direct SERS	Apple	0.038; linear 0.05–1.00 $\text{mg kg}^{-1}$	Ranging 0.02–5 $\text{mg kg}^{-1}$ (EU MRL depending each kind of apples)	205
Chlorpyrifos (CPF), pyrimethanil (PYR)	Citrate AuNP colloid	Direct SERS; spectra classified & quantified with MC-CNN-GRU deep learning	Fruit surfaces (apples, strawberries)	2.0 × 10 <sup>-4</sup> $\text{mg cm}^{-2}$ (CPF), 1.2 × 10 <sup>-4</sup> $\text{mg cm}^{-2}$ (PYR); linear 0.0002–0.20 $\text{mg cm}^{-2}$	Area-based LOD; not directly comparable to $\text{mg per kg MRL}$	200
Thiram	AgNP hydrogel	AgNPs embedded in soft gel pressed to fruit/vegetable surfaces to pick up analyte	Apple, tomato, pepper peels	2 $\text{pg cm}^{-2}$ (apple), 140 $\text{pg cm}^{-2}$ (tomato/pepper); linear 2–1000 $\text{pg cm}^{-2}$	Area-based LOD; not directly comparable to $\text{mg per kg MRL}$	203
Deltamethrin	AuNP colloid	Direct SERS	Soil	0.056 $\text{mg kg}^{-1}$ (soil); linear 0.056–5 $\text{mg kg}^{-1}$	No soil MRL	206
Carbofuran	AuNP colloid	Direct SERS	Soil	0.053 $\text{mg kg}^{-1}$ (soil); linear 0.053–5 $\text{mg kg}^{-1}$	No soil MRL	206
Dimethoate, omethoate	AgNP colloid	Direct SERS, KNO <sub>3</sub> -induce aggregation to create hot spots	Agricultural water, olive leaves	5 × 10 <sup>-7</sup> M (~0.115 $\text{mg L}^{-1}$ ); linear 0.115–100 $\text{mg L}^{-1}$	No agricultural water MRL	201
Methyl parathion	Au nanorod array	Anisotropic NPs + NP arrangement	Lake water; fruit/leaf swabs	1 $\mu\text{M}$ (~0.263 $\text{mg L}^{-1}$ ) in water; linear 0.263–26.3 $\text{mg L}^{-1}$ (water); 110–440 $\text{ng cm}^{-2}$ (surfaces); linear 110–1000 $\text{ng cm}^{-2}$ (surface)	No agricultural water MRL	201

Table 6 (Contd.)

Analytes	SERS substrate	Strategy	Real sample	LOD/range	Permissible limit <sup>191,192</sup>	Ref.
Fonofos, phosmet, sulfoxaflo	AuNP colloid	Direct SERS; chemometric models (KNN, SVM, PLSR) classify & quantify	Paddy/agricultural water	Fonofos 0.5 mg L <sup>-1</sup> ; linear 0.5–50 mg L <sup>-1</sup> ; phosmet 0.25 mg L <sup>-1</sup> ; linear 0.25–25 mg L <sup>-1</sup> ; Sulfoxaflo 1 mg L <sup>-1</sup> ; linear 1–100 mg L <sup>-1</sup>	No agricultural water MRL	202
<b>Other contaminants</b>						
Silver nanoparticles (AgNPs)	AgNPs in the sample	Triple-functional surfactant ligand for particle binding to create hot spots, and SERS reporting	Wheat tissue extracts (wheat leaves)	2 µg AgNPs per g wheat; 100 ng L <sup>-1</sup> in aqueous samples	No official plant tissue limit	207
PFAS (PFOA & PFOS)	Ag nanorod (AgNR) array	Surface functionalization with cysteine/6-MCH to promote adsorption; chemometric detection <i>via</i> SVM/SVR	Environmental water	1 ppt (PFOA); 4:28 ppt (PFOS)	4 ppt (US EPA) for both PFOA and PFOS	209
Microplastics (PS, PP, PET)	Ring-shaped Au nanogap array	Label-free detection based on polymer Raman fingerprints	Tap water, bottled water wash	50-nm PS: 1 µg mL <sup>-1</sup> PP & PET: Identified qualitatively	No established MRL	208

sensors for pesticides detection in plant and soil are listed in Table 6.

Many pesticides possess functional groups such as -SH, -COOH, or -NH<sub>3</sub>, which readily interact with metallic nanoparticle surfaces through chemisorption. This inherent affinity often allows them to be sensed using direct SERS, without any additional substrate functionalization, while still achieving impressive sensitivity (Table 6). In addition to this sensitivity, researchers have desired to boost selectivity of the sensors, allowing them to detect multiple targets as in real-world condition. For fruit surfaces, extraction combined with data-assisted analysis, as in the citrateAuNP system coupled to a multi-channel convolutional neural network (MC-CNN) combined with a gated recurrent unit (GRU) (MC-CNN-GRU) deep learning model, enables simultaneous detection and quantification of multiple residues such as chlorpyrifos and pyrimethanil, even in the presence of overlapping Raman features.<sup>200</sup> Meanwhile, more advanced engineered nanostructures, such as ordered Au nanorod arrays, enhance electromagnetic coupling for analytes like methyl parathion in lake water and on plant surfaces,<sup>201</sup> while chemometric-assisted colloidal SERS platforms allow classification and quantification of multiple pesticides in paddy water, addressing the reality of multi-residue usage in crop protection.<sup>202</sup> For more convenient sample collection, stamp-like AgNPs hydrogels were fabricated, achieving ultra-low detection limits for thiram directly on produce peels without the need for destructive sample preparation.<sup>203</sup> Recent studies intend to detect pesticides on the surface of fruit or leave in the effort of developing invasive detection, however, their area-based LODs and linear ranges were not directly comparable to established mg per kg MRLs.<sup>200,203</sup> Using plant extracts as real samples, other studies resulted in linear ranges covering the established MRLs (Table 6).<sup>204,205</sup> For soil, solvent extraction followed by AuNP colloidal SERS has been applied to monitor deltamethrin and carbofuran at ~0.05 mg kg<sup>-1</sup>, a sensitivity level appropriate for guiding application rates despite the absence of formal soil MRLs.<sup>206</sup> Also, current assessments for water often default to the EU Drinking Water Directive threshold for individual pesticides (0.1 µg L<sup>-1</sup>), which is designed for potable water rather than irrigation or process water. As a result, many SERS studies on agricultural water, despite achieving µg L<sup>-1</sup>-level sensitivity and clear utility for on-site screening, cannot be formally benchmarked against a relevant regulatory value for cultivation-stage monitoring. This gap underscores the need for matrix-specific guidance values to fully contextualize method performance in pre-harvest pesticide control.

**4.3.3. Other contaminants.** In addition to pesticides and heavy metal ions, a range of other contaminants in soil and water can adversely impact crop productivity and environmental health before cultivation. These include engineered NPs from agricultural inputs and industrial runoff, pharmaceutical residues from wastewater irrigation, microplastics, and persistent organic pollutants (POPs) such as polychlorinated biphenyls (PCBs) and polycyclic aromatic hydrocarbons (PAHs). Detecting these contaminants at trace levels is essential for effective soil and water management, as their accumulation can



alter soil microbiota, disrupt nutrient cycling, and cause long-term ecological risks. SERS offers a rapid, sensitive, and minimally invasive approach for monitoring such emerging pollutants in complex matrices, enabling timely intervention to ensure safe and sustainable agricultural practices from the outset of the cultivation cycle.

Engineered nanoparticles, such as AgNPs, have been detected in wheat tissues through a triple-functional surfactant ligand strategy that facilitates particle binding, achieving LODs down to  $2 \mu\text{g g}^{-1}$  in plant tissue and  $100 \text{ ng L}^{-1}$  in water.<sup>207</sup> For other contaminants, to overcome weak adsorption and low Raman cross-sections of target analytes, integration of selective surface chemistries or/and nanostructure geometries have been generated. For example, nanoplastic detection has advanced using ring-shaped Au nanogap substrates using nanosphere lithography and adhesion lithography as shown in Fig. 5b. The 20-nm nanogaps allowing polymer-specific fingerprinting of polystyrene (PS), polypropylene (PP), and polyethylene terephthalate (PET) in drinking water and bottle wash residues, with sensitivity to 50-nm PS particles at  $1 \mu\text{g mL}^{-1}$  without the assistance of any coating agents.<sup>208</sup> For persistent organic pollutants like per- and polyfluoroalkyl substances (PFAS), Ag nanorod arrays-based sensors were fabricated. The authors co-assembled cysteine and 6-mercapto-1-hexanol (6-MCH) to create a surface with both charged functional groups (from cysteine) and hydrophilic, less sterically hindered regions (from 6-MCH). This enhances adsorption of polar, amphiphilic PFAS molecules like perfluorooctanoic acid (PFOA) and perfluorooctane sulfonate (PFOS) onto the Ag nanorod substrate, which otherwise have weak affinity for bare metal surfaces. It was then coupled with machine learning algorithms to achieve an LOD down to 1 ppt for PFOA, which is even lower than the maximum contaminant level requirements of United States Environmental Protection Agency (U.S. EPA).<sup>209</sup> The LOD value of PFOS, however, is 4.28 ppt, which is slightly higher than US EPA drinking water limits. Thus, the sensors should be further improved for more effective results.

Across cultivation stages, SERS has moved from opportunistic demos to targeted tools that can flag contamination at decision-relevant levels, providing the chemistry matches the matrix. For heavy metals, direct SERS is rare but feasible for oxyanions (*e.g.*, arsenate/arsenite on tailored Ag surfaces); most successes use indirect schemes (chromogenic ligands, MOFs, DNazymes, magnetic capture) that convert weak scatterers into robust spectral readouts and routinely reach  $\text{sub-}\mu\text{g L}^{-1}$  to  $\text{ng L}^{-1}$  in water, often surpassing drinking-water or irrigation benchmarks. For pesticides, many molecules adsorb strongly enough for direct SERS, and field-lean formats (stamp/tape gels, ordered films) push area-based detection on peels and leaves, while chemometric/machine-learning pipelines deconvolve overlaps for multi-residue calls; where studies report extract-based assays, linear ranges around MRLs are achievable, but surface LODs still need consistent unit mapping to regulatory metrics. A broader class of emerging contaminants, such as engineered nanoparticles, microplastics, PFAS/POPs, benefits from affinity engineering (polymer/thiol co-monolayers, nanogap architectures) to overcome weak adsorption, delivering size/chemistry-specific

fingerprints and, for some PFAS, ppt-level limits. Recurrent constraints are matrix fluorescence, adsorption competition, and cross-study comparability; the fixes echo elsewhere in the review: selective interfaces up front, matrix-matched or standard-addition calibration, ratiometric or internal-standard quantitation, and explicit reporting of geometry and baseline parameters so performance can be judged against relevant regulatory thresholds rather than idealized lab conditions.

#### 4.4. Pathogens

During cultivation and pre-harvest stages, timely detection of plant pathogens is essential to prevent disease outbreaks, minimize crop losses, and maintain product quality. Conventional diagnostic techniques, such as culture-based assays, ELISA, and polymerase chain reaction (PCR) are highly sensitive but often require extensive sample preparation, skilled personnel, and centralized laboratory facilities, resulting in delays that limit their utility for rapid, in-field decision-making.<sup>210,211</sup> SERS offers a powerful alternative, enabling rapid, label-free, and ultrasensitive detection of pathogen-specific biomarkers, including nucleic acids, proteins, metabolites, and structural components.<sup>212</sup> Integrating SERS-based sensing into cultivation and pre-harvest monitoring supports precision agriculture by enabling early interventions to contain disease spread and ensure crop health prior to harvest. Various strategies have been developed to improve analytical performance and practical deployment of pathogen SERS sensors. First, to overcome matrix interference from plant tissues, stemming from pigments, lignin, cellulose, and secondary metabolites, Kim *et al.* mitigated spectral overlap in *Pseudomonas syringae* pv. *actinidiae* (Psa) analysis by modifying nanostructured Ag electrodes with iodide and  $\text{Ca}^{2+}$ , which enhanced bacterial cell adsorption and reduced nonspecific plant-derived signals. Moreover, electrochemically assisted SERS for Psa detection improved cell capture efficiency on the electrode surface, thereby increasing the probability of pathogen detection without nucleic acid amplification.<sup>213</sup> In another study, in *Valsa mali* detection from apple bark, Fang *et al.* employed chemometric models based on SERS spectroscopy with PCA, competitive adaptive reweighted sampling (CARS) and random frog (RFrog) variable selection, together with back-propagation artificial neural network (BP-ANN), extreme learning machine (ELM), random forest (RForest) and least squares support vector machine (LS-SVM) classification, to separate healthy, early- and late-diseased spectra, enabling >90% classification accuracy despite strong plant backgrounds.<sup>214</sup> Besides, the low pathogen concentration during early infection stages is a challenge in the effort of improving SERS performance of the sensors because the pathogen load may be below the detection threshold for label-free SERS. This was addressed by Lau *et al.*, who integrated recombinase polymerase amplification (RPA) with SERS nanotags for *Botrytis cinerea*, *P. syringae* and *Fusarium oxysporum*. RPA enables rapid, isothermal amplification of pathogen DNA, eliminating the need for thermal cycling and making the method suitable for on-site use. The entire reaction is performed in one tube, simplifying workflow and reducing contamination risk. This platform demonstrated outstanding sensitivity, detecting as



Table 7 Several SERS sensors for pathogens in plants

Analytes	SERS substrate	Strategy	Real sample/context	LOD/Accuracy	Ref.
<i>Pseudomonas syringae</i> pv. actinodiae (Psa; kiwifruit canker)	Iodide- and Ca <sup>2+</sup> -modified nanostructured Ag electrode	Direct EC-SERS of intact bacterial cells; electrochemical potential enhances adsorption & spectral resolution	Pure cultures (method developed for plant leaf exudates)	Rapid, label-free; clear fingerprint spectra; species-specific discrimination	213
<i>Valsa mali</i> (apple valsa canker)	AuNP-based flexible SERS substrate + portable Raman	Direct spectral fingerprinting + chemometrics (PCA, CARS, BP-ANN, LS-SVM, etc.); SERS imaging to map lesion chemistry	Naturally infected apple bark	>90% classification accuracy for healthy vs. early vs. late stage; changes in cellulose/lignin signatures detected	214
<i>Botrytis cinerea</i> , <i>P. syringae</i> , <i>Fusarium oxysporum</i>	AuNP SERS nanotags with DNA probes + RPA amplification in field cartridge	Indirect nucleic acid hybridization; multiplex detection in portable setup	Infected <i>Arabidopsis</i> leaves & commercial tomato plants	LOD: 2 DNA copies ( <i>B. cinerea</i> ); <30 min total assay; simultaneous multiplex	215
<i>Phytophthora ramorum</i> (sudden oak death)	Planar Ag SERS chip with adenine-free DNA capture probes	LATE-PCR amplification of <i>Ypt1</i> → hybridization readout by SERS	Infected rhododendron leaves	Species-specific detection from leaf DNA without sequencing	216
Bacterial cells in planta (method demonstration)	AuNPs functionalized with 3-mercaptophenylboronic acid (3-MPBA)	Boronic acid–diol interaction with bacterial cell walls; SERS imaging to localize	Bacteria spiked into plant tissues; microscopy-guided SERS mapping	Chemical imaging of bacteria inside plant matrices	218
Tobacco mosaic virus (TMV)	Ag@Au nanostars functionalized with modified DNA strands in agar hydrogel	Nucleic acid hybridization	Tobacco leaves	Identifying infected leaves at different stages vs. healthy ones	217

few as two DNA copies, within 30 minutes (Fig. 5c).<sup>215</sup> In addition to sensitivity, selectivity has been concerned when detecting pathogens in plant to avoid false positives. Yüksel *et al.* demonstrated species-specific detection of *Phytophthora ramorum* directly from rhododendron leaves by coupling Linear-After-The-Exponential PCR (LATE-PCR) amplification with adenine-free DNA capture probes on a planar Ag SERS chip.<sup>216</sup> In a recent study, DNA probes were also employed to enhance selectivity of a SERS sensor for tobacco mosaic virus. The measurements were performed directly on tobacco leaves despite the interferences of various organic compounds inside the leaves. The study allowed identifying infected leaves at different stages and healthy ones.<sup>217</sup> In another approach, Hickey & He functionalized AuNPs with 3-MPBA to selectively bind bacterial cell wall diols, enabling SERS imaging of bacteria within plant tissues.<sup>218</sup>

For plant pathogens, SERS has shifted from proof-of-concept to deployable workflows that prioritize early, on-site decisions. Two complementary routes dominate. Label-free SERS leverages surface conditioning (iodide layers, divalent cations) and capture geometries (nanostructured electrodes, electrochemically assisted loading) to suppress plant-matrix backgrounds and increase cell adhesion, enabling direct spectral discrimination with chemometric models at field-relevant concentrations. Tag-based SERS couples sequence-specific recognition (aptamers/DNA probes) or rapid isothermal amplification (RPA/LATE-PCR) with robust SERS reporters to push sensitivity to ultralow copy numbers in closed-tube formats suited to the field. Crucially, NIR acquisition and shifted-excitation Raman difference spectroscopy (SERDS) (dual, closely spaced excitations around 785 nm) further tame pigment fluorescence and ambient light on intact tissues, improving separability of pathogen signatures during daylight measurements and in pigmented hosts. Practical gains come from three choices: (i) front-end enrichment (magnetic capture, electrodeposition, tissue-proximal sampling) to overcome low pathogen loads; (ii) background management (iodide conditioning, SERDS/NIR, transparent baseline preprocessing) to isolate pathogen bands from lignocellulosic and pigment signals; and (iii) validation with interpretable metrics (cross-validated accuracy, LOD in CFU or copies, matrix-matched recovery) that map to pre-harvest decisions. The result is a toolkit that can triage symptomatic and presymptomatic tissues, guide targeted interventions, and integrate with IPM without the turnaround of centralized assays. Table 7 summarizes several SERS-based sensors developed for detecting bacteria and viruses in plants.

## 5. Operational bottlenecks and remedies for field-deployable SERS

### 5.1. Recurrent bottlenecks

Field-deployable SERS in crops is capped by five recurrent bottlenecks: optical background (fluorescence/daylight), hot-spot stochasticity, substrate stability, matrix-limited quantitation, and sampling/geometry variance. Leaf and fruit pigments (chlorophylls, carotenoids, anthocyanins) and soil humics generate broad, drifting fluorescence under visible excitation



that buries weak Raman bands, which are most severely below 700 nm. We address fluorescence/daylight backgrounds, hot-spot variance, substrate aging, matrix effects, and geometry/sampling variance with targeted remedies in Section 5.2. Beyond background light, reproducibility is limited by hot-spot stochasticity (nanogap scatter, clustering) and by focus/standoff variation, which together inflate relative standard deviation at three levels: within-map, chip-to-chip, and batch-to-batch. Ordered, wafer-scale architectures consistently reduce spatial variance across centimeter-scale areas compared with randomly roughened films, and are therefore preferred when quantitative performance is the goal. Once sensitivity and spatial uniformity are addressed, substrate stability becomes the next bottleneck. Silver provides high enhancement but is chemically fragile: in realistic aqueous/ionic media similar to irrigation water, leaf rinsates, and soil slurries, AgNPs readily oxidize/sulfidize to Ag<sub>2</sub>S, degrading plasmonic response.<sup>219</sup> In agricultural SERS, this chemical aging recurs as a dominant failure mode; practical mitigation (surface conditioning, bimetallic shelling, and protective storage/handling) is detailed later. Ultimately, quantitation is constrained by matrix effects. Leaf saps, rinsates, irrigation/runoff, and soil slurries differ in ionic strength and pH and contain sugars, phenolics, proteins, and surfactants that compete for adsorption and reshape the interfacial double layer. Buffer-only calibration therefore overestimates performance; best practice in crop-control analytics converges on matrix-matched or standard-addition calibration near MRLs, with recoveries and bias explicitly reported. Moreover, most variance actually enters before illumination, such as sampling footprint and dwell, elution volume and time, headspace geometry, and ambient light. Accordingly, the next section specifies fixed-geometry optics and daylight-robust acquisition, and then formalizes matrix-aware calibration and reporting so that performance metrics remain meaningful outside the lab.

## 5.2. Operational remedies and standard operating procedures (SOPs)

**5.2.1. Surface stabilization.** Robust optical performance begins with interfacial control. Many surface modification approaches have been studied, allowing improvements in SERS performance. For example, a short iodide conditioning of Ag surface on the order of a millimolar KI dip for tens of seconds, followed by a rinse and dry, acts like a quick “surface cleaning” step. It strips weakly adsorbed contaminants, damps metal photoluminescence, and leaves more uniform adsorption sites. Multiple studies reported higher SERS signals and more stable calibration after this step, including quantitative work on the insecticide deltamethrin and broader tests showing the specific activating effect of I<sup>-</sup> on Ag-based SERS.<sup>220</sup> Because halides can also reorganize interfacial adsorption, the recipe should be kept constant across batches and applied before analyte exposure when chemistry allows. This simple consistency step pays off as lower variance downstream.<sup>221</sup>

For deployments that must survive humidity, rinsing, or weeks in storage, bimetallic core–shells provide a sturdier alternative. For example, coating silver with a nanometer-thin

Au skin (Ag@Au) preserves the strong near-fields while greatly improving chemical stability. Dendritic Ag@Au substrates have maintained SERS activity for months with negligible loss, whereas bare Ag analogues oxidized/sulfidized and faded. Mechanistic and follow-up studies agreed: the Au overlayer passivated the surface chemistry that killed enhancement while leaving the electromagnetic hot spots essentially intact.<sup>222</sup>

Conditioning layers (*e.g.*, halides) and protective skins (*e.g.*, ultrathin Au, silica) can slightly shift plasmon bands or trim raw EF. For transferability, it is necessary to report the chemistry, concentration, contact time, and when applied relative to analyte exposure, and note any spectral/EF change. Long-horizon durability and sustainability considerations are consolidated in Section 6.5.

**5.2.2. Precision engineering & ratiometry.** Quantitative precision comes from pattern-defined, wafer-scale substrates that fix hot-spot architecture so centimeter-scale maps are consistent. Once geometric uniformity is established, ratiometry (built-in internal standards) turns intensity into robust ratios that ride out day-to-day/site-to-site drift. Large-area, pattern-defined arrays that are identical across the surface suppress spatial variance before any chemometric processing. Once geometric uniformity is established, ratiometry provides the next layer of robustness. Embedding a built-in internal standard (IS) turns intensity into a ratio  $R = I_{\text{analyte}}/I_{\text{IS}}$  that rides out day-to-day and site-to-site drift. In a pesticide-oriented example, a large-scale self-assembled Au@4-MBA@Ag array placed the reporter 4-MBA between gold and silver, so every spectrum carried its own yardstick; the authors report point-to-point RSD = 8.84% and batch-to-batch RSD = 14.97%, with higher calibration accuracy for thiram and thiabendazole after ratiometric correction than without it.<sup>57</sup> Where 4-MBA would overlap target bands, label-free IS choices exist, for example, purine as an intrinsic, non-overlapping calibrant, so ratiometry remains available even when pesticides or plant metabolites sit near common reporter bands.<sup>223</sup> A practical caveat is that thiol-rich exudates or aged Ag can displace surface reporters, biasing  $R$  during extended field work; checking IS-band stability and refreshing the reporter when drift appears minimizes this effect.

Transferability beyond a single lab is strongest when precision is quantified at three distinct levels: RSD<sub>within</sub> (map-level, same chip), RSD<sub>between</sub> (chip-to-chip within a batch), and RSD<sub>batch</sub> (across fabrication runs). Contemporary quantitation practice follows the same scaffold: uniform substrate design to curb spatial variance, ratiometry to stabilize calibration slopes, and transparent figures of merit ( $R^2$ , LOD/LOQ definitions, bias/recovery) so others can reproduce your calibration in real matrices.<sup>224</sup>

**5.2.3. Background control (optics & cleanup).** Under strong pigment/humic backgrounds and daylight, optical control is the primary lever. For intact leaves, an 830 nm leaf-clip fixes the probe-leaf standoff, blocks stray light, and logs operating power of about 130 mW, yielding stable on-leaf spectra in greenhouse/field conditions.<sup>225</sup> For soils in daylight, shifted-excitation Raman difference spectroscopy (SERDS) with a dual-wavelength source around 785 nm (*e.g.*, 785.2 and 784.6 nm)



removes shared fluorescence and ambient light while preserving the Raman signal. As a result, field deployments have resolved nine mineral classes and recovered soil organic carbon under daylight.<sup>226,227</sup>

Simplifying the chemistry that drives fluorescence often yields the largest gains. In plant extracts and rinse solutions, removing pigments upstream of measurement proves effective: a QuEChERS-lite cleanup (salt-out followed by dispersive SPE with PSA/C18 and graphitized carbon black) has been paired with handheld SERS for crop-residue analysis and has pushed LODs below regulatory MRLs in real rice matrices. In practice, this single pass removes much of the chromophore and surfactant load while preserving target analytes for rapid readout.<sup>228</sup> When color persists, a short TLC/HPTLC separation followed by SERS on the isolated band physically decouples analyte from the fluorescent streak. Carbendazim, for example, has been cleanly detected from kale leaves and orange juice using diatomite TLC plates as the separation stage prior to SERS interrogation, illustrating a generally useful “separate-then-enhance” workflow for leaf/fruit matrices.<sup>229</sup> For non-destructive plant phenotyping, headspace routes bypass aqueous pigments entirely: adsorbent-SERS/headspace-capture architectures collect leaf VOCs on a sorbent, then read by SERS, a format demonstrated on living and dried plant material and compatible with field deployments where GC-MS is impractical.<sup>80</sup>

Waters used in agriculture (irrigation, runoff) challenge SERS twice: humic/fulvic substances both fluoresce and compete for adsorption. A small-volume activated-carbon/SPE pre-step is a pragmatic fix borrowed from water analytics; decades of work show activated carbon efficiently removes dissolved natural organic matter, including humic fractions that dominate color and background, improving downstream quantitation even when the detector is not SERS-specific.<sup>230</sup> Recent reports likewise engineer carbons for pesticide removal at trace levels, underscoring that carbon pretreatment is compatible with analyte preservation when conditions are tuned.<sup>231</sup> When soils are processed as slurries, a brief dilute-settle-filter step can reduce humics and particulates and yield manageable baselines. For *in situ* daylight measurements, SERDS as outlined above is advisable.

Chemical cleanup and dilution curb fluorescence but can also strip the surface-active fraction that drives SERS at low doses, flattening calibration slopes near decision thresholds.

**5.2.4. Sampling geometry & field quality assurance and quality control (QA/QC).** Most day-to-day variances are geometric and temporal. For intact leaves, a fixed-standoff, light-blocking leaf-clip geometry (as described above) stabilizes acquisition. For surface residues on fruit or leaf cuticles, documenting the sampled area (cm<sup>2</sup>), contact pressure and duration, and elution volume and time constrains variability. Flexible paste-and-peel or tape-based SERS methods establish a constant footprint and, when footprint and dwell are specified, yield reproducible recoveries on curved produce; swab-extract workflows show similar consistency when swab area and solvent volumes are fixed.<sup>232</sup>

For plant VOCs, the headspace functions as a small, well-defined reactor: chamber volume, temperature, and equilibration time are specified before adsorption or SERS readout. Headspace solid-phase microextraction papers and plant-focused, adsorbent-based headspace capture followed by SERS show that fixing these three parameters stabilizes intensity ratios and classification.<sup>233</sup> For soils measured *in situ*, documentation of ambient-light control (a light shroud *versus* SERDS as mentioned in the previous section) clarifies comparability. Finally, field quality assurance and quality control (QA/QC) should include regular blanks and duplicates (for example, one QC sample per 10–20 samples) recorded with the same geometry and timing as real samples to make precision measurable rather than assumed.

**5.2.5. Matrix-aware calibration & preprocessing.** Quantitative accuracy degrades when calibration is performed in a matrix cleaner than the sample. In crops and waters, salts, humic substances, sugars, phenolics, and surfactants alter adsorption and band ratios; accordingly, calibration in the intended measurement matrix is preferred. Official control practice has converged on matrix-matched curves or standard addition at or near the decision limit, with recoveries and bias reported explicitly, because buffer-only calibration systematically overestimates performance in plant-derived matrices.<sup>234</sup> Ratiometric SERS complements this approach by converting intensity to a ratio,  $R = I_{\text{analyte}}/I_{\text{IS}}$ , which reduces day-to-day and site-to-site drift (*e.g.*, an Au@4-MBA@Ag array that maintained stable precision across positions and batches while preserving accurate pesticide quantitation).<sup>57</sup> A complementary route embeds a stable Raman indicator within the MIP layer to decouple weak intrinsic Raman from quantitation, which demonstrated for protein biomarkers and conceptually applicable to matrix-rich agricultural assays where intrinsic signals are faint.<sup>235</sup> Extending this idea, a reporter-inspector architecture (RRIM) on protein-PDA has been shown to reduce nonspecific binding and support quantitative readout in complex samples; while demonstrated in protein systems, the selectivity mechanism is relevant to colored, interference-prone agricultural matrices.<sup>109</sup> Baseline handling merits the same discipline: reproducibility improves when a documented, fluorescence-robust algorithm is applied with reported parameters. Common choices include asymmetric least squares (AsLS) and adaptive iteratively reweighted penalized least squares (airPLS).<sup>236,237</sup>

In field use, external calibration is often optimistic (slope compression, intercept shifts). Matrix matching or standard addition near the decision level is preferred, despite added time on leaves. Isotopologue/analog reporters can diverge in adsorption in high-salt extracts. Headspace SERS is constrained by partitioning and capture time in humid air. Chemometric models should report external-set error from day/site-separate data to guard against leakage and domain shift. Even with imprinting, template aging, site heterogeneity, and leachables can bias calibration; these pitfalls are documented for molecular-imprinting optical sensors and should be checked in outdoor workflows.<sup>238</sup>



**5.2.6. Storage & shelf-life.** Silver gives high enhancement but ages in humid, sulfur-bearing environments. Thin Au skins on Ag (Ag@Au) preserve near-field strength while improving chemical stability; dendritic Ag@Au has maintained SERS activity for roughly six months, whereas bare Ag analogues degraded.<sup>222</sup> Vacuum-sealed storage similarly limits oxidative aging; flexible Ag-based films stored in sealed bags retained performance and spatial uniformity. For field kits, store flexible films and paper/tape substrates sealed against air, humidity, and UV (with desiccant when feasible).<sup>234</sup> Report shelf life at defined checkpoints (0/30/60 days) with any LSPR shift and enhancement-factor change; broader sustainability/affordability guidance appears in Section 6.5.

## 6. Translation to agricultural decisions, validation, and sustainability

Decision-relevant SERS in agriculture rests on three pillars: clearly defined endpoints, disciplined validation, and sustainable substrates and workflows. Each is developed across crop quality, plant health, and environmental monitoring.

### 6.1. Crop-quality control: safety and intrinsic quality

For safety, SERS is used as a rapid screen for pesticide residues and other contaminants on leaves, peels, and whole produce, with performance referenced to commodity-specific maximum residue limits (MRLs). Sampling geometries are fixed and disclosed, such as clip, tape/paste-and-peel, or swab, with area (cm<sup>2</sup>), contact pressure/time, and elution volume/time specified to constrain variance. Flexible, fieldable sampling formats (paper/tape/films; swab-based SERS) are documented across recent studies.<sup>79–83,217</sup> Optical control under field illumination is addressed in portable/field SERS deployments.<sup>168,202,209</sup>

Intrinsic quality is treated as compositional profiling and authentication. Primary sugars and organic acids, pectin, and secondary metabolites that govern flavor, color, and nutrition (e.g., catechins, anthocyanins, capsaicinoids, vitamins) are measured in matrices that reflect use, such as juices, pulps, teas, and minimally processed extracts. Representative implementations are summarized in the article's application tables and case discussions. Calibration follows the same discipline as above. Quantitation follows matrix-matched or standard-addition calibration, with ratiometric internal standards and a documented baseline algorithm with fixed parameters, as detailed in Section 5.2.5; units are aligned to context (ng cm<sup>-2</sup> for surface residues; μM or mg L<sup>-1</sup> for extracts) and comparisons to regulatory MRLs (mg kg<sup>-1</sup>) are made only when a defensible area-to-mass conversion is stated, otherwise reported as screening results.

### 6.2. Plant health: stress phenotyping and pathogen surveillance

Targets include phytohormones (salicylic, jasmonic, abscisic acids), phenolics, and volatile organic compounds as early stress/disease indicators, and spores or cells on leaf and fruit surfaces for pathogen surveillance. Phytohormone roles and

representative SERS strategies are detailed in the article (e.g., derivatization-enabled detection of indole-3-butyric acid and broader hormone context).<sup>69,169</sup> VOC phenotyping uses head-space capture with SERS-active or SERS-read substrates; examples include 4-MPBA-AuNP capture of methyl salicylate, polymer-coated Ag nanoshells embedded in leaves for *in vivo* VOC mapping under field conditions, and adsorptive polymer-based collectors that discriminate caterpillar-induced plants from controls.<sup>80,167,168</sup> Conventional diagnostics (culture, ELISA, PCR) set the benchmark but face in-field constraints, which SERS aims to mitigate.<sup>210,211</sup> Pathogen-oriented implementations include recombinase polymerase amplification coupled to SERS nanotags with copy-level sensitivity in about 30 min, species-specific LATE-PCR on planar Au SERS chips, DNA-probe-guided detection of tobacco mosaic virus directly on leaves, and ligand-assisted SERS imaging of bacteria within plant tissues.<sup>215–218</sup> For hormone/VOC and pathogen readouts, calibration is matrix-matched or by standard addition and uses ratiometry with fixed baseline parameters, as specified in Section 5.2.5; results are reported in operational units (ng cm<sup>-2</sup>, copies or CFU mL<sup>-1</sup>) with method-appropriate benchmarks.

### 6.3. Water and soils: irrigation, runoff, and surface soils

In irrigation and runoff, SERS screening addresses pesticides and nutrients with respect to irrigation or potable-water guidance values.<sup>201,202</sup> For heavy metals, reported detection limits are benchmarked directly against World Health Organization (drinking water) and Food and Agriculture Organization (irrigation) thresholds.<sup>190,191</sup> For soils, two complementary modes are used. *In situ* optics under daylight support mineral fingerprints, soil-organic-carbon surrogates, and surface residues when the local matrix permits; slurry or extract measurements are used when extraction is unavoidable.<sup>206,226,227</sup> Water/soil assays use matrix-matched or standard-addition calibration with ratiometry and documented baseline settings, per Section 5.2.5; when needed, unit conversions to regulatory thresholds (e.g., μg L<sup>-1</sup> for water, mg kg<sup>-1</sup> for soils) are stated with assumptions.

### 6.4. Validation, comparability, and ruggedness

Transferability across farms, instruments, and seasons improves when precision is documented at three distinct levels: within-map repeatability on the same chip (RSD<sub>within</sub>), chip-to-chip precision within a fabrication batch (RSD<sub>between</sub>), and across-batch precision over independent fabrication runs (RSD<sub>batch</sub>). In practice, external validation on day- and site-separate sets often provides a more realistic view of performance (see Section 5.2.2).<sup>107,209</sup> Typical reporting includes the root mean squared error of prediction (RMSEP), bias, and 0.5×/1×/2× recoveries for regression,<sup>234</sup> and sensitivity, specificity, and the area under the receiver operating characteristic curve (AUROC) for blinded classification tests.<sup>215–218</sup> Ruggedness studies introduce controlled variation in temperature, humidity, illumination, operator, and storage age, with any shifts in slope or in the limit of detection/quantitation recorded; this framing aligns with the discussion of portability/



standardization gaps and chemometrics/ratiometry in quantitative SERS.<sup>202,209</sup> Multi-site trials on representative commodities and watersheds should use shared reference materials, harmonized preprocessing (baseline algorithm and parameters), and common analyte/internal-standard bands; inter-site precision and agreement with reference methods should be reported to demonstrate model transfer. For disease diagnostics, blinded sets spanning healthy, stressed, and infected states quantify sensitivity/specificity and the stability of classification across day/night and operator changes; nucleic-acid-assisted SERS implementations provide concrete templates (RPA-SERS; LATE-PCR on planar Au; DNA-probe virus detection; ligand-assisted in-planta imaging).<sup>215–218</sup> For nutrient and contaminant monitoring, recovery is characterized for the actual sampling media (swab, tape, headspace sorbent) and as a function of storage time between sampling and readout, consistent with flexible/tape/swab workflows.<sup>217</sup> Field QA/QC, regular field blanks and field duplicates at a stated cadence, should be implemented and documented so precision is measured rather than assumed.

### 6.5. Durability, sustainability, and affordability

Substrate choices should consider durability and environmental footprint. Silver delivers high enhancement but ages in humid, sulfur-bearing air; where practical, ultrathin Au skins or inert oxide/silica overlayers plus sealed storage help preserve near-fields. We encourage authors to report shelf-life at defined checkpoints (*e.g.*, 0/30/60 days) together with any resonance shift or change in enhancement factor. Evidence for scalable, precision fabrication that preserves uniformity (*e.g.*, UV-nanoimprint, roll-to-roll) is particularly helpful.<sup>239</sup> Flexible and encapsulated formats (PDMS, PEN, tapes) and their durability trade-offs are summarized in Table 3.

Affordability can be made transparent by summarizing: precious-metal loading, yield to functional substrate (after washing/ligand exchange), purification/solvent burden, process throughput and reject fraction, reuse cycles under stated packaging, and end-of-life recovery/recyclability. Where feasible, provide the order-of-magnitude cost per test and the mass of Au/Ag per test, together with support type and reuse cycles. When possible, favor cellulose/chitosan/silk supports and note end-of-life handling. A formal life-cycle assessment for agricultural SERS remains a gap and could be pursued alongside EF/RSD/LOD benchmarking. Practical field packaging against dust, UV, and moisture is also useful to document.

### 6.6. Data assets and reuse

Re-use and meta-analysis are enabled by curated spectral sets for each application class, including residues on commodity leaves/peels, headspace phenotyping under defined stressors, irrigation/runoff waters, and surface soils, with minimal meta-data (excitation wavelength, power at the sample, integration time, standoff, substrate batch and storage age, baseline method and parameters, analyte and internal-standard bands) and fixed train/test splits near decision thresholds. Large, open spectral libraries collected under realistic agricultural

conditions are encouraged to support adaptive models that remain accurate beyond their original training domain. Fabrication routes that support dataset comparability at scale (*e.g.*, nanoimprint/roll-to-roll) should be discussed in tandem with deployment considerations. For application anchors, Table 4 (stress markers), Table 5 (non-stress plant metabolites), and Table 6 (water/soil contaminants with WHO/FAO comparators) provide analyte–matrix pairs and LOD/range contexts relevant to dataset design.

In summary, the combination of controlled geometry and optics, stable surface chemistry, ratiometric quantitation, and matrix-aware calibration should convert laboratory sensitivity into decision-grade evidence for residue compliance, quality grading, early stress and disease calls, and water–soil monitoring, while validation and sustainability frameworks should keep conclusions comparable across instruments, sites, and seasons and enable deployment at scale.

## 7. Conclusions

SERS has progressed from isolated demonstrations to a materials-guided approach for agriculture. Mechanistic understanding of electromagnetic and charge-transfer contributions, together with control of hot-spot geometry and interfacial chemistry, now informs substrates ranging from noble-metal architectures to metal–semiconductor and metal-MOF hybrids, selective layers, and flexible/patterned formats. When aligned with the analyte and matrix, these designs support key agricultural tasks, including tracking intrinsic quality markers, phenotyping plant stress *via* hormones and VOCs, identifying pathogens, and screening contaminants in water, soils, and produce. Across these domains, we report the EF, LOD/LOQ, and RSD ranges observed in the literature and document common constraints including fluorescence/background, hot-spot variability, stability, and matrix interference. Looking ahead, progress hinges on tighter coupling between mechanism-aware design, matrix-aware operation, and transparent evaluation, alongside scalable, durable fabrication and clearer reporting. With these elements, SERS is well placed to deliver quantitative, comparable evidence for plant-health management, residue control, and crop-quality assurance.

## Author contributions

N. H. Anh: conceptualization, methodology, formal analysis, data curation, writing – original draft; D. T. N. Nga: formal analysis, investigation, data curation, writing – original draft; T. D. Cuong: formal analysis, methodology, writing – review & editing; M. Q. Doan: formal analysis, methodology, writing – review & editing; A. T. Le: conceptualization, methodology, supervision, project administration, writing – review & editing.

## Conflicts of interest

The authors confirm that no financial interests or personal relationships exist that could have influenced the findings presented in this paper.



## Data availability

This review does not generate new datasets or code. All data discussed are available in the published articles cited in the reference list.

## Acknowledgements

This work was financially supported by Phenikaa University under grant number PU2024-1-A-03. We also would like to acknowledge the A&A Green Phoenix Group JSC through Financial Supports for Purchasing Research Equipments of Key Research Group (NEB Lab). The authors would like to thank Assoc. Prof. Thanh Ha-Duong from ITODYS Laboratory, University Paris-Cité, for inspirations and interesting discussions.

## References

- 1 Y. Jia, L. Kang, Y. Wu, C. Zhou, D. Li, J. Li and C. Pan, *J. Agric. Food Chem.*, 2023, **71**, 13595–13611.
- 2 P. Punniyakotti, S. Vinayagam, R. Rajamohan, S. D. Priya, M. Moovendhan and T. Sundaram, *J. Environ. Chem. Eng.*, 2024, **12**, 113349.
- 3 X. T. Ju, C. L. Kou, P. Christie, Z. X. Dou and F. S. Zhang, *Environ. Pollut.*, 2007, **145**, 497–506.
- 4 P. Singh, P. C. Pandey, G. P. Petropoulos, A. Pavlides, P. K. Srivastava, N. Koutsias, K. A. K. Deng and Y. Bao, in *Hyperspectral Remote Sensing*, ed. P. C. Pandey, P. K. Srivastava, H. Balzter, B. Bhattacharya and G. P. Petropoulos, Elsevier, 2020, pp. 121–146, DOI: [10.1016/B978-0-08-102894-0.00009-7](https://doi.org/10.1016/B978-0-08-102894-0.00009-7).
- 5 A. Khan, U. Nawaz, A. Ulhaq and R. W. Robinson, *PLoS One*, 2020, **15**, e0243243.
- 6 S. M. Javidan, A. Banakar, K. Rahnama, K. A. Vakilian and Y. Ampatzidis, *Smart Agric. Technol.*, 2024, **8**, 100480.
- 7 *Laboratory Guide for Identification of Plant Pathogenic Bacteria*, ed. N. W. Schaad, J. B. Jones and W. Chun, American Phytopathological Society Press, St Paul, USA, 3rd edn, 2001, <http://www.scisoc.org>, US\$55, ISBN 089054 263 5 (paperback), John Wiley & Sons, Ltd, pp. 373.
- 8 M. F. Clark and A. N. Adams, *J. Gen. Virol.*, 1977, **34**, 475–483.
- 9 Y. M. Wang, B. Ostendorf, D. Gautam, N. Habili and V. Pagay, *Remote Sens.*, 2022, **14**, 1542.
- 10 G. U. Balcke, V. Handrick, N. Bergau, M. Fichtner, A. Henning, H. Stellmach, A. Tissier, B. Hause and A. Frolov, *Plant Methods*, 2012, **8**, 47.
- 11 X.-Z. Huang, J.-Y. Chen, H.-J. Xiao, Y.-T. Xiao, J. Wu, J.-X. Wu, J.-J. Zhou, Y.-J. Zhang and Y.-Y. Guo, *Sci. Rep.*, 2015, **5**, 11867.
- 12 H. Yu, Y. Zhang, K. A. G. Wyckhuys, K. Wu, X. Gao and Y. Guo, *Environ. Entomol.*, 2010, **39**, 600–609.
- 13 M. Zhu, X. Huang, L. Liu and H. Shen, *Talanta*, 1997, **44**, 1407–1412.
- 14 Y. Cui, Q. Ge, P. Zhao, W. Chen, X. Sang, Y. Zhao, Q. Chen and H. Wang, *Front. Plant Sci.*, 2021, **12**, 2021.
- 15 O. Fiehn, *Curr. Protoc. Mol. Biol.*, 2016, **114**, 31–32.
- 16 Y. Fu, T. Liu, X. Wang, Y. Wang, Q. Gong, G. Li, Q. Lin and S. Zhu, *Front. Plant Sci.*, 2023, **14**, 2023.
- 17 S. Pang, T. Yang and L. He, *TrAC, Trends Anal. Chem.*, 2016, **85**, 73–82.
- 18 X. X. Han, R. S. Rodriguez, C. L. Haynes, Y. Ozaki and B. Zhao, *Nat. Rev. Methods Primers*, 2022, **1**, 87.
- 19 Y. Xu, Q. Dong, S. Cong and Z. Zhao, *Analysis Sensing*, 2024, **4**, e202300067.
- 20 R. S. Das and Y. K. Agrawal, *Vib. Spectrosc.*, 2011, **57**, 163–176.
- 21 R. R. Jones, D. C. Hooper, L. Zhang, D. Wolverson and V. K. Valev, *Nanoscale Res. Lett.*, 2019, **14**, 231.
- 22 D. Wolverson, in *Characterization of Semiconductor Heterostructures and Nanostructures*, ed. C. Lamberti, Elsevier, Amsterdam, 2008, pp. 249–288, DOI: [10.1016/B978-0-444-53099-8.00008-7](https://doi.org/10.1016/B978-0-444-53099-8.00008-7).
- 23 V. Smeliková, I. Kopal, M. Člupek, M. Dendisová and M. Švecová, *Anal. Chem.*, 2024, **96**, 5416–5427.
- 24 K. Ashiagbor, H. Jayan, N. Yosri, N. K. Amaglo, X. Zou and Z. Guo, *Food Chem.*, 2025, **463**, 141394.
- 25 P. Yu, L. Ma, X. Yang, S. Xue, Z. Zhang, L. Sun and J. Cai, *ACS Omega*, 2025, **10**, 25158–25175.
- 26 S.-Y. Wang, X.-C. Shi, G.-Y. Zhu, Y.-J. Zhang, D.-Y. Jin, Y.-D. Zhou, F.-Q. Liu and P. Laborda, *Trends Food Sci. Technol.*, 2021, **116**, 583–602.
- 27 A. I. Pérez-Jiménez, D. Lyu, Z. Lu, G. Liu and B. Ren, *Chem. Sci.*, 2020, **11**, 4563–4577.
- 28 S. L. Kleinman, E. Ringe, N. Valley, K. L. Wustholz, E. Phillips, K. A. Scheidt, G. C. Schatz and R. P. Van Duyne, *J. Am. Chem. Soc.*, 2011, **133**, 4115–4122.
- 29 A.-I. Henry, T. W. Ueltschi, M. O. McAnally and R. P. Van Duyne, *Faraday Discuss.*, 2017, **205**, 9–30.
- 30 R. L. McCreery, in *Raman Spectroscopy for Chemical Analysis*, John Wiley & Sons, Inc., 2000, pp. 15–33, DOI: [10.1002/0471721646.ch2](https://doi.org/10.1002/0471721646.ch2).
- 31 K. M. Kosuda, J. M. Bingham, K. L. Wustholz, R. P. Van Duyne and R. J. Groarke, in *Comprehensive Nanoscience and Nanotechnology*, ed. D. L. Andrews, R. H. Lipson and T. Nann, Academic Press, Oxford, 2nd edn, 2016, pp. 117–152, DOI: [10.1016/B978-0-12-803581-8.00611-1](https://doi.org/10.1016/B978-0-12-803581-8.00611-1).
- 32 S.-Y. Ding, J. Yi, J.-F. Li, B. Ren, D.-Y. Wu, R. Panneerselvam and Z.-Q. Tian, *Nat. Rev. Mater.*, 2016, **1**, 16021.
- 33 R. Aroca, in *Surface-Enhanced Vibrational Spectroscopy*, John Wiley & Sons, Ltd, England, 2006, ch. 4, pp. 107–132, DOI: [10.1002/9780470035641.ch4](https://doi.org/10.1002/9780470035641.ch4).
- 34 M. Moskovits, *Phys. Chem. Chem. Phys.*, 2013, **15**, 5301–5311.
- 35 L. Jensen, C. M. Aikens and G. C. Schatz, *Chem. Soc. Rev.*, 2008, **37**, 1061–1073.
- 36 S. Cong, X. Liu, Y. Jiang, W. Zhang and Z. Zhao, *Innovation*, 2020, **1**, 100051.
- 37 H. K. Lee, Y. H. Lee, C. S. L. Koh, G. C. Phan-Quang, X. Han, C. L. Lay, H. Y. F. Sim, Y.-C. Kao, Q. An and X. Y. Ling, *Chem. Soc. Rev.*, 2019, **48**, 731–756.
- 38 D. Radziuk and H. Moehwald, *Phys. Chem. Chem. Phys.*, 2015, **17**, 21072–21093.



- 39 L.-A. Wu, W.-E. Li, D.-Z. Lin and Y.-F. Chen, *Sci. Rep.*, 2017, **7**, 13066.
- 40 K. A. E. Jebakumari, N. K. Murugasenapathi and T. Palanisamy, *Biosensors*, 2023, **13**, 102.
- 41 T.-S. Ko and Y.-L. Chen, *Nanomaterials*, 2022, **12**, 786.
- 42 S. I. Siddiqui and S. A. Chaudhry, *J. Cleaner Prod.*, 2019, **223**, 849–868.
- 43 G. Morris, I. Sorzabal-Bellido, M. Bilton, K. Dawson, F. McBride, R. Raval, F. Jäckel and Y. A. Diaz Fernandez, *Nanomaterials*, 2021, **11**, 1580.
- 44 Y. Kumar, A. S. K. Sinha, K. D. P. Nigam, D. Dwivedi and J. S. Sangwai, *Nanoscale*, 2023, **15**, 6075–6104.
- 45 S. M. Mousavi, S. A. Hashemi, V. Rahmanian, M. Y. Kalashgrani, A. Gholami, N. Omidifar and W.-H. Chiang, *Biosensors*, 2022, **12**, 466.
- 46 L. Mehrvar, M. Sadeghipari, S. H. Tavassoli, S. Mohajerzadeh and M. Fathipour, *Sci. Rep.*, 2017, **7**, 12106.
- 47 J. Chen, Y. Li, K. Huang, P. Wang, L. He, K. R. Carter and S. R. Nugen, *ACS Appl. Mater. Interfaces*, 2015, **7**, 22106–22113.
- 48 O. S. Muddineti, B. Ghosh and S. Biswas, *Int. J. Pharm.*, 2015, **484**, 252–267.
- 49 R. A. Sperling and W. J. Parak, *Philos. Trans. R. Soc., A*, 2010, **368**, 1333–1383.
- 50 Y. Teng, Z. Wang, W. Huang and Y. She, *Vib. Spectrosc.*, 2022, **120**, 103381.
- 51 Y. Kou, X.-G. Zhang, H. Li, K.-L. Zhang, Q.-C. Xu, Q.-N. Zheng, J.-H. Tian, Y.-J. Zhang and J.-F. Li, *Anal. Chem.*, 2024, **96**, 4275–4281.
- 52 R. Akter, T. Kim, J. S. Choi and H. Kim, *Biosensors*, 2025, **15**, 153.
- 53 G. C. Olar, L. C. Cotet, L. Baia, A. Mihis and M. Baia, *Mater. Today: Proc.*, 2021, **45**, 4096–4099.
- 54 M. Aghili, B. T. Hogan, J. P. Chamberland, D. P. J. Barz and A. Docoslis, *ACS Omega*, 2025, **10**, 19175–19188.
- 55 G. Chen, M. Guan, Z. Yang, F. Mi, Y. Wang and X. Rao, *Microchem. J.*, 2024, **207**, 112098.
- 56 J. Yang, M. Pan, X. Yang, K. Liu, Y. Song and S. Wang, *Food Chem.*, 2022, **395**, 133623.
- 57 K. Wang and J. Li, *Spectrochim. Acta, Part A*, 2021, **263**, 120218.
- 58 T. T. Ha Pham, X. H. Vu, N. D. Dien, T. T. Trang, T. T. Kim Chi, P. H. Phuong and N. T. Nghia, *RSC Adv.*, 2022, **12**, 7850–7863.
- 59 N. Abu Bakar and J. G. Shapter, *Heliyon*, 2023, **9**, e14686.
- 60 K. O. Ay, G. Dikmen and O. Koyuncu, *J. Mol. Struct.*, 2024, **1297**, 136869.
- 61 R. Nisticò, P. Rivolo, C. Novara and F. Giorgis, *Colloids Surf., A*, 2019, **578**, 123600.
- 62 S. L. Kleinman, R. R. Frontiera, A.-I. Henry, J. A. Dieringer and R. P. Van Duyne, *Phys. Chem. Chem. Phys.*, 2013, **15**, 21–36.
- 63 F. Schuknecht, K. Kołataj, M. Steinberger, T. Liedl and T. Lohmueller, *Nat. Commun.*, 2023, **14**, 7192.
- 64 J. Wang, J. Fu, H. Chen, A. Wang, Y. Ma, H. Yan, Y. Li, D. Yu, F. Gao and S. Li, *Biosens. Bioelectron.*, 2023, **224**, 115051.
- 65 K. Song, W. Xue, X. Li, Y. Chang and M. Liu, *Anal. Chem.*, 2024, **96**, 8830–8836.
- 66 H. A. Nguyen, I. Jupin, P. Decorse, S. Lau-Truong, S. Ammar and N.-T. Ha-Duong, *RSC Adv.*, 2019, **9**, 32296–32307.
- 67 D. Oliveira, M. C. C. G. Carneiro and F. T. C. Moreira, *Microchim. Acta*, 2024, **191**, 238.
- 68 Y. Zhang, L. Li, H. Zhang, J. Shang, C. Li, S. M. Z. A. Naqvi, Z. Birech and J. Hu, *Anal. Bioanal. Chem.*, 2022, **414**, 2757–2766.
- 69 F. Wang, X. Gu, C. Zheng, F. Dong, L. Zhang, Y. Cai, Z. You, J. You, S. Du and Z. Zhang, *Anal. Chem.*, 2017, **89**, 8836–8843.
- 70 Y. Tian, L. Cong, H. Sun, W. Wei, F. Wu, F. Li, G. Xu and W. Niu, *ACS Appl. Nano Mater.*, 2024, **7**, 20308–20316.
- 71 D. Radziuk, R. Schuetz, A. Masic and H. Moehwald, *Phys. Chem. Chem. Phys.*, 2014, **16**, 24621–24634.
- 72 S. Van Vu, A.-T. Nguyen, A.-T. Cao Tran, V.-H. Thi Le, T. N. H. Lo, T. H. Ho, N. N. T. Pham, I. Park and K. Q. Vo, *Nanoscale Adv.*, 2023, **5**, 5543–5561.
- 73 W. Zhang, H. Zhang, J. Li, X. Zou, W. Wang, H. Hu, K. Iqbal, P. Zhou and W. Ye, *Microchim. Acta*, 2023, **191**, 1.
- 74 M. Q. Doan, N. H. Anh, N. X. Quang, N. X. Dinh, D. Q. Tri, T. Q. Huy and A.-T. Le, *J. Electron. Mater.*, 2022, **51**, 150–162.
- 75 K. Wang, D.-W. Sun, H. Pu and Q. Wei, *Talanta*, 2021, **223**, 121782.
- 76 K. A. Maleeva, I. E. Kaliya, A. P. Tkach, A. A. Babaev, M. A. Baranov, K. Berwick, T. S. Perova, A. V. Baranov and K. V. Bogdanov, *Materials*, 2022, **15**, 5197.
- 77 Q. Wang, C. Zhang, T. Gong, W. Kong, W. Yue, W. Chen, Z. Xie, Y. Su and L. Li, *Opt. Commun.*, 2019, **444**, 56–62.
- 78 L. Wu, H. Zhou, W. He, B. Yu and L. Qian, *Surf. Interfaces*, 2022, **32**, 102156.
- 79 S. M. Kong, D. Shin, J.-W. Oh, H. Park, J. S. Lee, N.-I. Won and Y. H. Na, *Chem. Eng. J.*, 2023, **471**, 144753.
- 80 J. Park, J. A. Thomasson, C. C. Gale, G. A. Sword, K.-M. Lee, T. J. Herrman and C. P. C. Suh, *ACS Omega*, 2020, **5**, 2779–2790.
- 81 H. Wu, C. Kanike, A. Marcati and X. Zhang, *Langmuir*, 2024, **40**, 4218–4227.
- 82 Q. D. Mai, H. A. Nguyen, N. X. Dinh, N. T. Thu Thuy, Q. H. Tran, P. C. Thanh, A.-T. Pham and A.-T. Le, *Talanta*, 2023, **253**, 124114.
- 83 H. A. Nguyen, Q. D. Mai, D. T. Nguyet Nga, M. K. Pham, Q. K. Nguyen, T. H. Do, V. T. Luong, V. D. Lam and A.-T. Le, *Nanoscale Adv.*, 2024, **6**, 3106–3118.
- 84 D. T. N. Nga, Q. D. Mai, L. H. T. Nguyen, T. L. H. Doan, V. Thi Kim Oanh, T. Ngoc Bach, V. Dinh Lam, H. A. Nguyen and A.-T. Le, *RSC Adv.*, 2025, **15**, 4915–4925.
- 85 D. T. Nguyet Nga, Q. D. Mai, N. Le Nhat Trang, M. K. Pham, N. Q. Hoa, V. D. Lam, H. Van Tuan, H. A. Nguyen and A.-T. Le, *Phys. Chem. Chem. Phys.*, 2023, **25**, 17496–17507.
- 86 A. J. Haes, C. L. Haynes, A. D. McFarland, G. C. Schatz, R. P. Van Duyne and S. Zou, *MRS Bull.*, 2005, **30**, 368–375.
- 87 P. K. Jain, X. Huang, I. H. El-Sayed and M. A. El-Sayed, *Acc. Chem. Res.*, 2008, **41**, 1578–1586.
- 88 K. Rhee, A. Tukova, M. Tavakkoli Yarakhi and Y. Wang, *Nanoscale*, 2023, **15**, 2087–2095.



- 89 M. Li, S. K. Cushing and N. Wu, *Analyst*, 2015, **140**, 386–406.
- 90 J. Tao, Y. Lu, J. Chen, D. Lu, C. Chen, P. Wang and H. Ming, *Plasmonics*, 2011, **6**, 785–789.
- 91 C. J. Orendorff, L. Gearheart, N. R. Jana and C. J. Murphy, *Phys. Chem. Chem. Phys.*, 2006, **8**, 165–170.
- 92 R. Taheri-Ledari, M. R. Ahghari, F. Ansari, M. Forouzandeh-Malati, S. S. Mirmohammadi, S. Zarei-Shokat, S. Ramezanzpour, W. Zhang, Y. Tian and A. Maleki, *Nanoscale Adv.*, 2022, **4**, 4418–4433.
- 93 S. J. Lee, H. Jang and D. N. Lee, *Nanoscale Adv.*, 2023, **5**, 5165–5213.
- 94 R. N. Revnic, G. F. Ştiufiuc, V. Toma, A. Onaciu, A. Moldovan, A. B. Ţigu, E. Fischer-Fodor, R. Tetean, E. Burzo and R. I. Ştiufiuc, *Int. J. Mol. Sci.*, 2022, **23**, 8830.
- 95 M. J. Oliveira, P. Quaresma, M. Peixoto de Almeida, A. Araújo, E. Pereira, E. Fortunato, R. Martins, R. Franco and H. Águas, *Sci. Rep.*, 2017, **7**, 2480.
- 96 L. Ignatane, R. Ignatans, J. Prikulis, A. Trausa, C. F. Tipaldi, E. Vanags, M. Zubkins, K. Smits and A. Sarakovskis, *Nanomaterials*, 2024, **14**, 1784.
- 97 A. Arbuz, A. Sultangazyev, A. Rapikov, Z. Kunushpayeva and R. Bukasov, *Nanoscale Adv.*, 2022, **4**, 268–280.
- 98 O. Rabin and S. Y. Lee, *J. Nanotechnol.*, 2012, **2012**, 870378.
- 99 W. Fang, S. Jia, J. Chao, L. Wang, X. Duan, H. Liu, Q. Li, X. Zuo, L. Wang, L. Wang, N. Liu and C. Fan, *Sci. Adv.*, 2019, **5**, eaau4506.
- 100 T. Köker, N. Tang, C. Tian, W. Zhang, X. Wang, R. Martel and F. Pinaud, *Nat. Commun.*, 2018, **9**, 607.
- 101 L. Zheng, F. Hu, Y. Zhao, J. Zhu, X. Wang, M. Su and H. Liu, *J. Agric. Food Chem.*, 2023, **71**, 20793–20800.
- 102 H.-l. Hao, J. Zhu, G.-j. Weng, J.-j. Li, Y.-b. Guo and J.-w. Zhao, *ACS Sens.*, 2024, **9**, 942–954.
- 103 R. Tang, R. A. Hughes, W. J. Tuff, A. Corcoran and S. Neretina, *Nanoscale Adv.*, 2024, **6**, 3632–3643.
- 104 D.-K. Lim, K.-S. Jeon, J.-H. Hwang, H. Kim, S. Kwon, Y. D. Suh and J.-M. Nam, *Nat. Nanotechnol.*, 2011, **6**, 452–460.
- 105 M. Kim, S. M. Ko, J.-M. Kim, J. Son, C. Lee, W.-K. Rhim and J.-M. Nam, *ACS Cent. Sci.*, 2018, **4**, 277–287.
- 106 R. Cheng, D. Jia, Z. Du, J.-X. Cheng and C. Yang, *RSC Adv.*, 2023, **13**, 27321–27332.
- 107 S. Weng, X. Hu, J. Wang, L. Tang, P. Li, S. Zheng, L. Zheng, L. Huang and Z. Xin, *J. Agric. Food Chem.*, 2021, **69**, 2950–2964.
- 108 C. Liu, D. Xu, X. Dong and Q. Huang, *Trends Food Sci. Technol.*, 2022, **128**, 90–101.
- 109 X. Chen, A. Ostovan, M. Arabi, Y. Wang, L. Chen and J. Li, *Anal. Chem.*, 2024, **96**, 6417–6425.
- 110 Y. Yin, C. Li, Y. Yan, W. Xiong, J. Ren and W. Luo, *Coatings*, 2022, **12**, 360.
- 111 S. Cong, Y. Yuan, Z. Chen, J. Hou, M. Yang, Y. Su, Y. Zhang, L. Li, Q. Li, F. Geng and Z. Zhao, *Nat. Commun.*, 2015, **6**, 7800.
- 112 W. Yang, J. Tang, Q. Ou, X. Yan, L. Liu and Y. Liu, *ACS Omega*, 2021, **6**, 27271–27278.
- 113 X. He, Y. Gong, L. Niu and C. Li, *Nanomaterials*, 2025, **15**, 521.
- 114 W. A. Tegegne, W.-N. Su, M.-C. Tsai, A. B. Beyene and B.-J. Hwang, *Appl. Mater. Today*, 2020, **21**, 100871.
- 115 W. Yin, S. An, T. Cheng, L. Jiang and Y. Cao, *Appl. Surf. Sci.*, 2024, **672**, 160820.
- 116 J. Ye, R. Arul, M. K. Nieuwoudt, J. Dong, T. Zhang, L. Dai, N. C. Greenham, A. Rao, R. L. Z. Hoye, W. Gao and M. C. Simpson, *J. Phys. Chem. Lett.*, 2023, **14**, 4607–4616.
- 117 D. Glass, E. Cortés, S. Ben-Jaber, T. Brick, R. Quesada-Cabrera, W. J. Peveler, Y. Zhu, C. S. Blackman, C. R. Howle, I. P. Parkin and S. A. Maier, *Proc. SPIE*, 2019, **11010**, 110100D.
- 118 Q. D. Mai, H. A. Nguyen, T. L. H. Phung, N. Xuan Dinh, Q. H. Tran, T. Q. Doan, A. T. Pham and A.-T. Le, *ACS Appl. Nano Mater.*, 2022, **5**, 15518–15530.
- 119 D. Glass, E. Cortés, S. Ben-Jaber, T. Brick, W. J. Peveler, C. S. Blackman, C. R. Howle, R. Quesada-Cabrera, I. P. Parkin and S. A. Maier, *Adv. Sci.*, 2019, **6**, 1901841.
- 120 K. Abid, N. H. Belkhir, S. B. Jaber, R. Zribi, M. G. Donato, G. Di Marco, P. G. Gucciardi, G. Neri and R. Maàlej, *J. Phys. Chem. C*, 2020, **124**, 20350–20358.
- 121 S. Almohammed, F. Zhang, B. J. Rodriguez and J. H. Rice, *Sci. Rep.*, 2018, **8**, 3880.
- 122 L.-J. Gu, C.-L. Ma, X.-H. Zhang, W. Zhang, S. Cong and Z.-G. Zhao, *Chem. Commun.*, 2018, **54**, 6332–6335.
- 123 J. Zhou, J. Zhang, H. Yang, Z. Wang, J.-a. Shi, W. Zhou, N. Jiang, G. Xian, Q. Qi, Y. Weng, C. Shen, Z. Cheng and S. He, *Nanoscale*, 2019, **11**, 11782–11788.
- 124 Q.-Q. Chen, R.-N. Hou, Y.-Z. Zhu, X.-T. Wang, H. Zhang, Y.-J. Zhang, L. Zhang, Z.-Q. Tian and J.-F. Li, *Anal. Chem.*, 2021, **93**, 7188–7195.
- 125 Q. Shao, D. Zhang, C.-e. Wang, Z. Tang, M. Zou, X. Yang, H. Gong, Z. Yu, S. Jin and P. Liang, *J. Phys. Chem. C*, 2021, **125**, 7297–7304.
- 126 N. L. N. Tran, L. H. Tho, N. Q. Tran, H. K. T. Ta, B. T. Phan, N. N. T. Pham, T. L. H. Doan and N. H. T. Tran, *Mater. Adv.*, 2024, **5**, 4401–4408.
- 127 Y. Pan, W. Wang, S. Guo, S. Jin, E. Park, Y. Sun, L. Chen and Y. M. Jung, *Chemosensors*, 2021, **9**, 111.
- 128 M. Kasztelan, A. Studzinska, G. Z. Żukowska and B. Pałys, *Front. Chem.*, 2021, **9**, 2021.
- 129 M. Yu, C. Qin, Z. Yu, B. Sun, D. Ni, D. Zhang and P. Liang, *Chemosensors*, 2024, **12**, 82.
- 130 Y. Liu, H. Ma, X. X. Han and B. Zhao, *Mater. Horiz.*, 2021, **8**, 370–382.
- 131 Y. Gu, S. Wu, Z. Luo, L. L. Lin and J. Ye, *Spectrochim. Acta, Part A*, 2024, **322**, 124852.
- 132 B. V. Ranishenka, A. Y. Panarin, I. A. Chelnokova, S. N. Terekhov, P. Mojzes and V. V. Shmanai, *Beilstein J. Nanotechnol.*, 2021, **12**, 902–912.
- 133 E. Hahm, D. Jeong, M. G. Cha, J. M. Choi, X.-H. Pham, H.-M. Kim, H. Kim, Y.-S. Lee, D. H. Jeong, S. Jung and B.-H. Jun, *Sci. Rep.*, 2016, **6**, 26082.
- 134 W.-I. K. Chio, S. Moorthy, J. Perumal, D. U. S, I. P. Parkin, M. Olivo and T.-C. Lee, *J. Mater. Chem. C*, 2020, **8**, 7051–7058.
- 135 W. Hu, L. Xia, Y. Hu and G. Li, *Anal. Chem.*, 2025, **97**, 1347–1356.



- 136 A.-q. Yang, D. Wang, X. Wang, Y. Han, X.-b. Ke, H.-j. Wang, X. Zhou and L. Ren, *RSC Adv.*, 2015, **5**, 38354–38360.
- 137 Y. Hu, S. Feng, F. Gao, E. C. Y. Li-Chan, E. Grant and X. Lu, *Food Chem.*, 2015, **176**, 123–129.
- 138 M. Arabi, A. Ostovan, Y. Wang, R. Mei, L. Fu, J. Li, X. Wang and L. Chen, *Nat. Commun.*, 2022, **13**, 5757.
- 139 R. K. Sinha, *Plasmonics*, 2023, **18**, 241–253.
- 140 Y. Choi, C. S. Jeon, K. B. Kim, H.-J. Kim, S. H. Pyun and Y. M. Park, *Talanta*, 2023, **260**, 124590.
- 141 D. Cialla-May, A. Bonifacio, T. Bocklitz, A. Markin, N. Markina, S. Fornasaro, A. Dwivedi, T. Dib, E. Farnesi, C. Liu, A. Ghosh and J. Popp, *Chem. Soc. Rev.*, 2024, **53**, 8957–8979.
- 142 S. Mahanty, S. Majumder, R. Paul, R. Boroujerdi, E. Valsami-Jones and C. Laforsch, *Sci. Total Environ.*, 2024, **950**, 174252.
- 143 Y. Chen, G. Mellot, D. van Luijk, C. Creton and R. P. Sijbesma, *Chem. Soc. Rev.*, 2021, **50**, 4100–4140.
- 144 W. Wang, Y. Chen, C. Xiao, S. Xiao, C. Wang, Q. Nie, P. Xu, J. Chen, R. You, G. Zhang and Y. Lu, *Chem. Eng. J.*, 2023, **474**, 145953.
- 145 W.-C. Huang, K.-F. Cheng and J.-Y. Shyu, *Nanoscale Adv.*, 2022, **4**, 1164–1172.
- 146 C. Wang, K. W. Wong, Q. Wang, Y. Zhou, C. Tang, M. Fan, J. Mei and W.-M. Lau, *Talanta*, 2019, **191**, 241–247.
- 147 S. Kumar, K. Namura, D. Kumaki, S. Tokito and M. Suzuki, *Results Mater.*, 2020, **8**, 100139.
- 148 B. Kim, H. Chun, S. J. Back and G. B. Jung, *J. Korean Phys. Soc.*, 2020, **76**, 1025–1028.
- 149 C. Zhang, P. Yi, L. Peng, X. Lai, J. Chen, M. Huang and J. Ni, *Sci. Rep.*, 2017, **7**, 39814.
- 150 M. Wu, C. Zhang, Y. Ji, Y. Tian, H. Wei, C. Li, Z. Li, T. Zhu, Q. Sun, B. Man and M. Liu, *Polymers*, 2020, **12**, 392.
- 151 J.-P. Peng, P.-J. Liu, Y.-T. Song, S.-Z. Zhao, X.-Y. Deng and Z.-K. Huang, *Chin. J. Polym. Sci.*, 2025, **43**, 1584–1591.
- 152 Z. Guo, Y. Zheng, C. Wang, H. Jayan, L. Yin, H. R. El-Seedi, Y. Gong and X. Zou, *Talanta*, 2025, **283**, 127168.
- 153 K. Ponlamuangdee, C. Rattanabut, N. Viriyakitpattana, P. Roeksrungruang, K. Karn-orachai, D. Pimalai and S. Bamrungsap, *Anal. Methods*, 2022, **14**, 1765–1773.
- 154 S. Jaitpal, S. R. Chavva and S. Mabbott, *ACS Omega*, 2022, **7**, 2850–2860.
- 155 D. Radziuk and H. Moehwald, *Nanoscale*, 2014, **6**, 6115–6126.
- 156 F. Usman, K. H. Ghazali, Y. W. Fen, F. Meriaudeau and R. Jose, *Eur. Polym. J.*, 2023, **195**, 112250.
- 157 R. d. Oliveira and A. C. Sant'Ana, *Chemosphere*, 2023, **338**, 139490.
- 158 M. Li, Y. Wei, X. Fan, G. Li, X. Tang, W. Xia, Q. Hao and T. Qiu, *JACS Au*, 2023, **3**, 468–475.
- 159 Q. Hao, Y. Chen, Y. Wei, G. Li, X. Tang, D. Chen, X. Zhu, L. Yao, X. Zhao, M. Li, J. Wang, X. Fan and T. Qiu, *J. Phys. Chem. Lett.*, 2024, **15**, 7183–7190.
- 160 W. Liu, X. Zhang, L. Liang, C. Chen, S. Wei and Q. Zhou, in *Reactive Oxygen Species and Oxidative Damage in Plants under Stress*, ed. D. K. Gupta, J. M. Palma and F. J. Corpas, Springer International Publishing, Cham, 2015, pp. 191–217, DOI: [10.1007/978-3-319-20421-5\\_8](https://doi.org/10.1007/978-3-319-20421-5_8).
- 161 J. E. Serrão, A. Plata-Rueda, L. C. Martínez and J. C. Zanoncio, *Sci. Nat.*, 2022, **109**, 17.
- 162 J. Peñuelas and J. Llusà, *Trends Ecol. Evol.*, 2004, **19**, 402–404.
- 163 P.-A. Lin, Y. Chen, G. Ponce, F. E. Acevedo, J. P. Lynch, C. T. Anderson, J. G. Ali and G. W. Felton, *Trends Plant Sci.*, 2022, **27**, 287–300.
- 164 S. Li, X. Yuan, Y. Xu, Z. Li, Z. Feng, X. Yue and E. Paoletti, *J. Environ. Sci.*, 2021, **108**, 152–163.
- 165 Z. Liu, M. Wang, M. Wu, X. Li, H. Liu, N. Niu, S. Li and L. Chen, *TrAC, Trends Anal. Chem.*, 2023, **158**, 116872.
- 166 Z. Li, Y. Liu, O. Hossain, R. Paul, S. Yao, S. Wu, J. B. Ristaino, Y. Zhu and Q. Wei, *Matter*, 2021, **4**, 2553–2570.
- 167 C. Song, Y. Wang, Y. Lei and J. Zhao, *J. Phys. Chem. C*, 2022, **126**, 772–778.
- 168 Y. S. Choi, W. K. Son, H. Kwak, J. Park, S. Choi, D. Sim, M. G. Kim, H. Kimm, H. Son, D. H. Jeong and S.-Y. Kwak, *Adv. Sci.*, 2025, **12**, 2412732.
- 169 A. Santner and M. Estelle, *Nature*, 2009, **459**, 1071–1078.
- 170 J. Cui, K. Hu, J.-J. Sun, L.-L. Qu and D.-W. Li, *Biosens. Bioelectron.*, 2016, **85**, 324–330.
- 171 C. Zaffino, B. Russo and S. Bruni, *Spectrochim. Acta, Part A*, 2015, **149**, 41–47.
- 172 G. Sarto, T. N. M. Cervantes, M. M. Slonski, J. V. Martins, P. C. Soto, H. de Santana and L. C. de Almeida, *Vib. Spectrosc.*, 2024, **134**, 103716.
- 173 E. Liu, L. Han, X. Fan, Z. Yang, Z. Jia, S. Shi, Y. Huang, L. Cai and X. Yuan, *Talanta*, 2022, **247**, 123552.
- 174 R. Mittler, S. I. Zandalinas, Y. Fichman and F. Van Breusegem, *Nat. Rev. Mol. Cell Biol.*, 2022, **23**, 663–679.
- 175 N. Smirnoff and D. Arnaud, *New Phytol.*, 2019, **221**, 1197–1214.
- 176 Z. Tan, C. Zhu, L. Han, X. Liao and C. Wang, *Sens. Actuators, B*, 2022, **373**, 132770.
- 177 J. Wu, K. Chen, J. Pan, D. Li, Y. Ma and N. Li, *Anal. Chem.*, 2024, **96**, 19981–19987.
- 178 L.-L. Qu, Y.-Y. Liu, S.-H. He, J.-Q. Chen, Y. Liang and H.-T. Li, *Biosens. Bioelectron.*, 2016, **77**, 292–298.
- 179 Y. Wang, C. Cheng, R. Ma, Z. Xu and Y. Ozaki, *Analyst*, 2022, **147**, 1815–1823.
- 180 H. Cao, H. Shi, J. Tang, Y. Xu, Y. Ling, X. Lu, Y. Yang, X. Zhang and H. Wang, *iScience*, 2023, **26**, 107821.
- 181 S. D. Iancu, A. Stefanu, V. Moisoiu, L. F. Leopold and N. Leopold, *Beilstein J. Nanotechnol.*, 2019, **10**, 2338–2345.
- 182 C. Camerlingo, M. Portaccio, R. Tatè, M. Lepore and I. Delfino, *Sensors*, 2017, **17**, 839.
- 183 A. I. Radu, M. Kuellmer, B. Giese, U. Huebner, K. Weber, D. Cialla-May and J. Popp, *Talanta*, 2016, **160**, 289–297.
- 184 J. Li, M. Zuo, W. Zhang, X. Zou and Z. Sun, *Food Anal. Methods*, 2022, **15**, 3468–3478.
- 185 D. Liu, J. Yang, S. Wen, M. Mu, W. Ji, B. Zhao, Y. Ozaki and W. Song, *Sens. Actuators, B*, 2024, **418**, 136251.
- 186 M. Qi, B. Wang, H. Jiang, Y. Li, P. Li, X. Zhang and L. Han, *J. Food Compos. Anal.*, 2024, **125**, 105740.



## Review

- 187 Y. Li, C. Zhao, C. Lu, S. Zhou, G. Tian, L. He, Y. Bao, M.-L. Fauconnier, H. Xiao and J. Zheng, *Food Chem.*, 2021, **338**, 128115.
- 188 B. H. Abdelmonem, L. T. Kamal, R. M. Elbaz, M. R. Khalifa and A. Abdelnaser, *Heliyon*, 2025, **11**, e41713.
- 189 Y. Yi, Y. Ma, F. Ai, Y. Xia, H. Lin and G. Zhu, *Chem. Commun.*, 2021, **57**, 7790–7793.
- 190 M. Mulvihill, A. Tao, K. Benjauthrit, J. Arnold and P. Yang, *Angew. Chem., Int. Ed.*, 2008, **47**, 6456–6460.
- 191 M. M. Orosun, S. Nwabachili, R. F. Alshehri, M. Omeje, I. F. Alshdroukhi, H. K. Okoro, C. O. Ogunkunle, H. Louis, F. A. Abdulhamid, S. E. Osahon, A. U. Mohammed, E. O. Ehinlafa, S. O. Yunus and O. Ife-Adediran, *Sci. Rep.*, 2023, **13**, 21220.
- 192 M. B. Pescod, Wastewater treatment and use in agriculture – FAO irrigation and drainage paper 47, *Food and Agriculture Organization of the United Nations*, Viale delle Terme di Caracalla, 00100 Rome, Italy, 1992.
- 193 B. Lv, Z. Sun, J. Zhang and C. Jing, *Colloids Surf., A*, 2017, **513**, 234–240.
- 194 S. S. R. Dasary, Y. K. Jones, S. L. Barnes, P. C. Ray and A. K. Singh, *Sens. Actuators, B*, 2016, **224**, 65–72.
- 195 C. Liu, H. Wang, S. Xu, H. Li, Y. Lu and C. Zhu, *Chemosensors*, 2023, **11**, 347.
- 196 W. Xu, A. Zhao, F. Zuo, R. Khan, H. M. J. Hussain and J. Li, *Anal. Bioanal. Chem.*, 2020, **412**, 4565–4574.
- 197 L. Szabó, L. F. Leopold, B. I. Cozar, N. Leopold, K. Herman and V. Chiş, *Cent. Eur. J. Chem.*, 2011, **9**, 410–414.
- 198 M. Hernández-Mesa and D. Moreno-González, *Separations*, 2022, **9**, 148.
- 199 J. Brinco, P. Guedes, M. Gomes da Silva, E. P. Mateus and A. B. Ribeiro, *Microchem. J.*, 2023, **195**, 109465.
- 200 Z. Chen, X. Dong, C. Liu, S. Wang, S. Dong and Q. Huang, *Sci. Rep.*, 2023, **13**, 19855.
- 201 A. W. Partridge, H. Y. Kaan, Y.-C. Juang, A. Sadruddin, S. Lim, C. J. Brown, S. Ng, D. Thean, F. Ferrer, C. Johannes, T. Y. Yuen, S. Kannan, P. Aronica, Y. S. Tan, M. R. Pradhan, C. S. Verma, J. Hochman, S. Chen, H. Wan, S. Ha, B. Sherborne, D. P. Lane and T. K. Sawyer, *Molecules*, 2019, **24**, 2292.
- 202 S. Weng, W. Zhu, R. Dong, L. Zheng and F. Wang, *Sensors*, 2019, **19**, 506.
- 203 A. L. Picone, M. L. Rizzato, A. R. Lusi and R. M. Romano, *Food Chem.*, 2022, **373**, 131570.
- 204 M. Han, H. Lu and Z. Zhang, *Molecules*, 2020, **25**, 4662.
- 205 F. Tunnisa, D. Nur Faridah, A. Afriyanti, D. Rosalina, M. Ana Syabana, N. Darmawan and N. Dewi Yuliana, *Food Chem.:X*, 2022, **14**, 100285.
- 206 Y. He, S. Xiao, T. Dong and P. Nie, *Int. J. Mol. Sci.*, 2019, **20**, 1731.
- 207 H. Guo, B. Xing, J. C. White, A. Mukherjee and L. He, *Analyst*, 2016, **141**, 5261–5264.
- 208 S. Luo, J. Zhang and J. C. de Mello, *Front. Bioeng. Biotechnol.*, 2023, **11**, 2023.
- 209 J. C. Rothstein, J. Cui, Y. Yang, X. Chen and Y. Zhao, *Sens. Diagn.*, 2024, **3**, 1272–1284.
- 210 M. M. López, E. Bertolini, A. Olmos, P. Caruso, M. T. Gorris, P. Llop, R. Penyalver and M. Cambra, *Int. Microbiol.*, 2003, **6**, 233–243.
- 211 F. Martinelli, R. Scalenghe, S. Davino, S. Panno, G. Scuderi, P. Ruisi, P. Villa, D. Stroppiana, M. Boschetti, L. R. Goulart, C. E. Davis and A. M. Dandekar, *Agron. Sustainable Dev.*, 2015, **35**, 1–25.
- 212 J. Perumal, Y. Wang, A. B. E. Attia, U. S. Dinish and M. Olivo, *Nanoscale*, 2021, **13**, 553–580.
- 213 L. Jiang, L. Luo, Z. Zhang, C. Kang, Z. Zhao, D. Chen and Y. Long, *Talanta*, 2024, **268**, 125336.
- 214 S. Fang, Y. Zhao, Y. Wang, J. Li, F. Zhu and K. Yu, *Front. Plant Sci.*, 2022, **13**, 2022.
- 215 H. Y. Lau, Y. Wang, E. J. H. Wee, J. R. Botella and M. Trau, *Anal. Chem.*, 2016, **88**, 8074–8081.
- 216 S. Yüksel, L. Schwenkbier, S. Pollok, K. Weber, D. Cialla-May and J. Popp, *Analyst*, 2015, **140**, 7254–7262.
- 217 L. N. Kissell, H. Liu, M. Sheokand, D. Vang, P. Kachroo and P. Strobbia, *ACS Sens.*, 2024, **9**, 514–523.
- 218 M. E. Hickey and L. He, *Talanta*, 2021, **225**, 122008.
- 219 C. Levard, E. M. Hotze, G. V. Lowry and G. E. Brown Jr, *Environ. Sci. Technol.*, 2012, **46**, 6900–6914.
- 220 Z. Hu, D. Peng, F. Xing, X. Wen, K. Xie, X. Xu, H. Zhang, F. Wei, X. Zheng and M. Fan, *Molecules*, 2023, **28**, 1700.
- 221 X. Song, X. Ren, D. Tang and X. Li, *Spectrochim. Acta, Part A*, 2022, **272**, 120950.
- 222 H. Jun Yin, Z. Yang Chen, Y. Mei Zhao, M. Yang Lv, C. An Shi, Z. Long Wu, X. Zhang, L. Liu, M. Li Wang and H. Jun Xu, *Sci. Rep.*, 2015, **5**, 14502.
- 223 H.-W. Cheng, H.-M. Tsai and Y.-L. Wang, *Anal. Chem.*, 2023, **95**, 16967–16975.
- 224 Y. Xu, W. Aljuhani, Y. Zhang, Z. Ye, C. Li and S. E. J. Bell, *Chem. Soc. Rev.*, 2025, **54**, 62–84.
- 225 S. Gupta, C. H. Huang, G. P. Singh, B. S. Park, N.-H. Chua and R. J. Ram, *Sci. Rep.*, 2020, **10**, 20206.
- 226 K. Sowoidnich, S. Vogel, M. Maiwald and B. Sumpf, *Appl. Spectrosc.*, 2022, **76**, 712–722.
- 227 K. Sowoidnich, S. Pätzold, M. Ostermann, B. Sumpf and M. Maiwald, *Analyst*, 2025, **150**, 2934–2944.
- 228 N. Logan, S. A. Haughey, L. Liu, D. T. Burns, B. Quinn, C. Cao and C. T. Elliott, *npj Sci. Food*, 2022, **6**, 3.
- 229 Z. Shen, Q. Fan, Q. Yu, R. Wang, H. Wang and X. Kong, *Spectrochim. Acta, Part A*, 2021, **247**, 119037.
- 230 F. Li, A. Yuasa, K. Ebie, Y. Azuma, T. Hagishita and Y. Matsui, *Water Res.*, 2002, **36**, 4592–4604.
- 231 B. Zieliński, P. Miądlicki and J. Przepiórski, *Sci. Rep.*, 2022, **12**, 20869.
- 232 J. Jiang, S. Zou, L. Ma, S. Wang, J. Liao and Z. Zhang, *ACS Appl. Mater. Interfaces*, 2018, **10**, 9129–9135.
- 233 C. Lancioni, C. Castells, R. Candal and M. Tascon, *Adv. Sample Prep.*, 2022, **3**, 100035.



- 234 X. Yan, H. Shi, P. Jia and X. Sun, *Nanomaterials*, 2022, **12**, 3894.
- 235 M. Arabi, A. Ostovan, Z. Zhang, Y. Wang, R. Mei, L. Fu, X. Wang, J. Ma and L. Chen, *Biosens. Bioelectron.*, 2021, **174**, 112825.
- 236 Z.-M. Zhang, S. Chen and Y.-Z. Liang, *Analyst*, 2010, **135**, 1138–1146.
- 237 M. Han, Y. Dang and J. Han, *Sensors*, 2024, **24**, 3161.
- 238 M. Arabi and L. Chen, *Langmuir*, 2022, **38**, 5963–5967.
- 239 K. Milenko, F. T. Dullo, P. C. V. Thrane, Z. Skokic and C. A. Dirdal, *Nanomaterials*, 2023, **13**, 1598.

